Molecular Photodetachment Spectrometry. I. The Electron Affinity of Nitric Oxide and the Molecular Constants of NO^- †

M. W. Siegel,* R. J. Celotta,‡ J. L. Hall,§ J. Levine,¶ and R. A. Bennett
Joint Institute for Laboratory Astrophysics, University of Colorado, Boulder, Colorado 80302
(Received 12 October 1971)

We apply laser photodetachment and photoelectron spectrometry for the first time to the study of molecular negative ions. We describe in detail the study of the nitric oxide ion NO^-; a following paper reports results for O_2^-. We use the NO^- results to develop and illustrate in detail the principles and applications of the technique. A mass-selected NO^- beam (680 eV) is crossed with a linearly polarized monochromatic (4880-Å) argon-ion laser beam, and electrons photodetached into a $4\pi/2000$-sr solid angle perpendicular to the crossed beams are energy analyzed using a hemispherical electrostatic monochromator. The data yield a set of vertical detachment energies between vibrational states of NO^- and NO, and relative intensities for these transitions. Angular distributions about the polarization direction are studied by rotating the laser polarization while maintaining the mutually perpendicular ion-beam–laser-beam–electron-collection geometry. For each transition we measure the anisotropy parameter β, corresponding to the form $[1+\beta P_2(\cos\theta)]$ for the angular distribution. Several arguments, including data on NO^{18-} photodetachment, are used to identify the initial and final vibrational states. Molecular rotational effects, and effects associated with the spin-orbit splitting of the final $NO(X\,^2\Pi)$ state are identified and included in the analysis. A Franck-Condon-factor analysis of the observed relative cross sections, parametrized by trial values of the NO^- molecular constants, is used to determine that for NO^- $\omega_e'' = 1470 \pm 200$ cm^{-1}, $r_e'' = 1.258 \pm 0.010$ Å, and $B_e'' = 1.427 \pm 0.02$ cm^{-1}. Using these constants, the measured vertical detachment energy is reduced by rotational and spin-orbit effects to the electron affinity $E_A(\mathrm{NO}) = 24^{+10}_{-5}$ meV.

I. INTRODUCTION

We have applied laser photodetachment[1–6] and photoelectron spectrometry[4] to the determination of molecular electron affinities[5,6] and molecular negative-ion spectroscopic constants. This paper and the following one describe, respectively, our results for the diatomic ions NO^- and O_2^-.

In this paper we describe the method, apparatus, theory, and analysis, with specific reference to the NO^- data and results. The following paper[7] deals with the specifics of the more complicated O_2^- case. By dividing the discussion in this way, we can use the clear, relatively simple NO^- results to illustrate the technique, general principles, and methods of analysis. The simplicity of these results has been of great value in pointing the way for us to extract maximum information from the data.

Because of the necessarily detailed nature of the arguments to be presented in Sec. II we feel that a short overview would be helpful.

The energy spectra of electrons photodetached from molecular negative ions will, in general, exhibit multiple peaks. The energy of each peak is essentially equal to the incident photon energy less the energy required to make the transition from the initial state of the negative ion to the final state of the neutral. A major problem is to identify correctly the initial and final vibrational states of these transitions. This problem is simplified in the NO^- case since we can show that only one initial vibrational state is present. The variation of transition intensities as a function of the final vibrational state determines, via the Franck-Condon[8] principle, that the initial state is the ground vibrational state.

We use three independent methods for assigning vibrational quantum numbers to the final states. One employs an accurate determination of the differences in energy between adjoining peaks in the electron energy spectrum. By comparing these differences with the known vibrational intervals in the neutral, we make a vibrational assignment. The second technique uses a Franck-Condon calculation and the relative transition intensities. The third method uses isotope substitution and measurement of the corresponding shift in vibrational energy levels.

The intensities of the various transitions are used, with the Franck-Condon principle, to yield a potential curve for the negative-ion state under study. The spectroscopic constants ω_e, r_e, and B_e of a negative-ion Morse potential are determined in this way. The value of B_e so obtained is used to correct for rotational effects which must be included in an accurate calculation of the electron affinity of the neutral.

As we use the term, the electron affinity of a molecule is the vertical detachment energy E_{vd}[6,9] between the rotational ground state of the negative

ion in its zeroth vibrational state and the corresponding rotational ground state of the neutral molecule in its zeroth vibrational state. Thus, the electron affinity is both a physical and an experimental observable.

II. METHOD

Let us briefly review the principles of the laser photodetachment technique for the determination of atomic electron affinities and photodetachment angular distributions, and then extend our discussion to the similar, but more detailed, molecular problem.

A negative-ion beam is crossed with a monochromatic linearly polarized laser photon beam. Photoelectrons ejected into a small (0.00628-sr) solid angle perpendicular to the crossed beams are collected and energy analyzed by a hemispherical electrostatic analyzer.[10,11] Rotatable laser polarization allows us to determine the photoelectron angular distribution[12,13] without mechanically changing the mutually perpendicular ion-beam–photon-beam–electron-collection geometry.

For simplicity in this discussion of the method, we suppose the initial atomic negative ion and the final atom have singlet ground states, and the negative ion has only one bound state. If the atomic ground state is the only level accessible by the laser photon energy, the photoelectron energy spectrum will show a single peak.

A. Kinematics

We first discuss the kinematics in the center of mass frame and later transform into the lab frame. The photon momentum $h\nu/c$ is easily seen to be negligible in comparison to the ion, atom, and electron momenta involved. Thus we write

$$h\nu = E_A + \Omega_0 + W_R , \tag{1}$$

$$(2\Omega_0 m)^{1/2} = (2W_R M)^{1/2}, \tag{2}$$

for conservation of energy and momentum, respectively, where m, M are the electron and final atom masses, and Ω_0 and W_R are the electron and atom recoil energies, respectively. Thus

$$h\nu = (1 + m/M)\,\Omega_0 + E_A . \tag{3}$$

Writing the ion mass as $m+M$, since the "mass equivalent of the electron affinity" is negligible, the transformation to the lab frame is accomplished by adding to the electron velocity vector the ion-beam velocity vector, of magnitude

$$U_{\text{beam}} = [2W/m+M]^{1/2} , \tag{4}$$

where W is the beam energy.

Reference to Fig. 1 gives

$$\frac{2\Omega_0}{m} = \frac{2\Omega_L}{m} + \frac{2W}{m+M} - 2\left(\frac{2\Omega_L}{m}\right)^{1/2} \times \left(\frac{2W}{m+M}\right)^{1/2} \cos(\tfrac{1}{2}\pi - \phi), \tag{5}$$

where ϕ is the electron direction, measured from a perpendicular to the beam, and Ω_L is the lab energy of the electron. As a consequence of this transformation an electron collected perpendicular to the ion beam must have been ejected in the center-of-mass frame backwards with respect to the beam direction with a velocity component equal to $-U_{\text{beam}}$. This effect is of importance both in determining electron affinities and vertical detachment energies, and in interpreting photodetachment angular distributions. Substituting Ω_0 as given by Eq. (3) into Eq. (4), after some rearrangement of terms, and eliminating terms of the order of $(m/M)\,\Omega_L$ and $(m/M)^2 W$, we obtain our main working equation

$$h\nu - E_A = \Omega_L + (m/M)\,W - 2(mW\Omega/M)^{1/2} \sin\phi . \tag{6}$$

The angularly dependent term is zero for collection perpendicular to the beam, and we henceforth, except in error-analysis considerations, omit it.

If the observed electron is, at some point be-

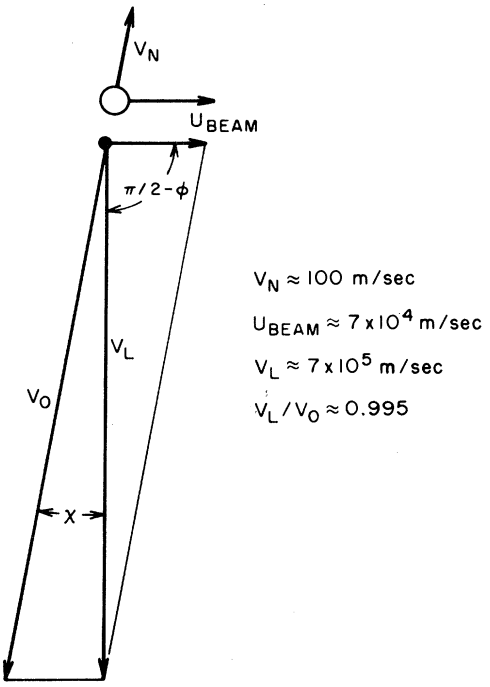

FIG. 1. Kinematics of photodetachment from an ion beam. Here U_{beam} is the ion-beam velocity, V_0 is the electron velocity in the center-of-mass system, V_L is the electron velocity measured by the electron monochromater, and V_N is the velocity of the recoiling neutral. ϕ measures the deviation from 90° of the angle formed by the electron-collection direction and the ion-beam direction. It is shown equal to zero in the figure. The numbers shown are typical for NO^- photodetachment.

tween photodetachment and detection, accelerated or decelerated by a difference in contact potential, then the observed Ω will be additively in error by the corresponding energy E_{cp}. Thus, we use $\Omega_L = \Omega + E_{cp}$, which gives

$$E_A = h\nu - \Omega - (m/M)W - E_{cp} \quad . \tag{7}$$

To eliminate the effect of this unknown contact-potential difference, all our electron affinities are measured with reference to an atom whose electron affinity is assumed known arbitrarily accurately, e.g., H^-,[14] or in these experiments O^-.[15] Since the reference ion is produced simultaneously with the unknown ion, and accelerated to the same final beam energy, we obtain

$$E_{A2} - E_{A1} = (\Omega_1 - \Omega_2) + mW(1/M_1 - 1/M_2) , \tag{8}$$

where subscripts 1 and 2 indicate the reference ion and the unknown ion, respectively. Equation (8) is the basis for all our energy measurements. Thus any future additive correction to the accepted value of the electron affinity of atomic oxygen, 1.465 ± 0.005 eV,[15] should similarly be added to all vertical detachment energies and electron affinites quoted herein.

B. Multiple States

Extension to multiple initial and final states is straightforward: Multiple states simply yield multiple peaks in the electron energy spectrum. For cases in which the multiplicity originates in spin-orbit splittings, the electron affinity is defined as the energy difference between the most strongly bound negative-ion level and the most strongly bound atomic level.[15] Thus the electron affinity of an atom may be larger than the photodetachment threshold of its negative ion.[16]

C. Angular Distributions

By rotating the laser polarization while observing the photodetachment rate we obtain the photoelectron angular distribution. Theory[13] and confirming experiments[12] have shown that, in general, for electric dipole transitions and linearly polarized light

$$\frac{d\sigma}{d\Omega} = \frac{\sigma_{tot}}{4\pi}\left[1 + \beta P_2(\cos\theta)\right], \tag{9}$$

where P_2 is the Legendre polynomial and θ is the angle between the electric field vector and the electron collection direction as measured in the plane containing the ion beam and the electron-collection direction. The angular distribution anisotropy parameter β is between $+1$ in the case of a pure $\cos^2\theta$ distribution and -2 in the case of a pure $\sin^2\theta$ distribution, and is given by a well-defined function[13,17] of the radial matrix elements connecting initial (bound) and final (free) electron states and the phase shifts of competing outgoing partial waves. In general two and only two partial waves contribute, corresponding to orbital angular momenta one unit more and one unit less than the initial bound electron angular momentum. We note that for atomic negative ions in which the detached electron originates in a p state and for photon energies on the order of 1 eV above threshold, the phase shifts for outgoing s and d waves frequently conspire to produce an angular distribution peaked perpendicular to the laser polarization peaked perpendicular to the laser polarization, i.e., $\beta \approx 1$.[12,13]

D. Extension to Molecular Photodetachment

Theoretical and experimental extension to molecular photodetachment[9,18] is straightforward, but introduces the complication of multiple photodetachment peaks corresponding to various initial-final vibrational state pairs. We have observed, for the first time, molecular negative-ion photodetachment electron energy spectra having this multipeaked structure.

The general kinematics of detachment and angular distributions are similar for atoms and molecules, and Eqs. (1)–(3) are directly applicable, with some changes in notation. As an extension of the usual notation for vibrational transitions in molecular absorption spectroscopy,[19] we denote the photodetachment transition between the negative-ion state $AB^-(v'', J'')$ and the neutral molecule state $AB(v', J')$ by $AB(v', J', v'', J'')AB^-$. For compactness, we usually omit the rotational-state designation, and write $AB(v', v'')AB^-$. Thus we must identify the photodetachment peak belonging to the transition $AB(0,0)AB^-$, whose energy is the zero-to-zero vertical detachment energy $E_{vd}(AB(0,0) \times AB^-)$, analogous to an atomic-electron affinity. However, the experimental $E_{vd}^T(AB(0,0)AB^-)$ is not equal to the molecular electron affinity: The electron affinity refers to the initial ion and final molecule in their ground rotational states.

E. Rotational Effects

The molecular ion beam has a rotational-state distribution which we characterize by a source temperature T. Therefore, although we define the molecular electron affinity as the energy difference between the lowest-lying states of the neutral and the ion, the vast majority of the transitions we observe will be between unresolved rotationally excited levels. Using the full notation we find

$$E_A(AB) \equiv \lim_{T_{vib} \to 0,\, T_{rot} \to 0} E_{vd}^T(AB(v', J', v'', J'')AB^-), \tag{10}$$

where T, v', and v'' are zero in the limit. In practice the electron affinity can be determined from photodetachment data only if the rotational tempera-

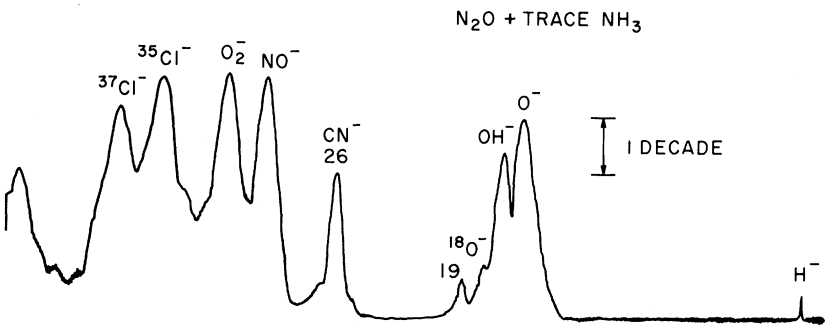

FIG. 2. Typical mass spectrum under the source conditions described in the text. The x axis is linear with mass and the y axis is logarithmic except near zero. A typical NO^- current is 10 nA.

ture of the ion beam is known and if B_e'' can be determined. Of course, this requirement applies to other than photodetachment methods too, but has not been taken into account for lack of knowledge of the rotational constant. The present experiment determines the molecular constant ω_e'' and r_e'', and thus B_e'', of the negative ion.

III. APPARATUS: HARDWARE AND DATA MANIPULATION

A. Source

Negative ions are produced by direct extraction from a glow-discharge source of the type described by Branscomb *et al.*[15] Typical operating conditions are 0.050 Torr of N_2O in the source, a discharge current of 2.5 mA, and a beam energy of 680 eV. Under these circumstances the beam in the interaction region consists of 20 nA each of NO^- and O_2^-, 60 nA of O^-, and a total of about 20 nA of various other negative ions. A typical mass spectrum is shown in Fig. 2. The use of off-axis extraction in the source results in a favorable initial ratio of ions to electrons (1:1000). Retarding potential analysis beyond the interaction region has shown a beam-energy spread of the order of 0.25 eV around the applied acceleration voltage. The details of the ion-production mechanisms have not been systematically investigated; however, there is good evidence that the efficient production of NO^- is highly dependent on how far the partially shielded 0.3-mm tungsten filament cathode protrudes into the discharge region.

B. Ion Optics and Mass Selection

Preliminary control of the beam is established by a large aperture (2-cm) einzel field lens (see Fig. 3). The ion beam is then electrostatically deflected through 10°, eliminating streaming neutrals and photons from the beam. A weak magnetic field removes the extracted electrons. The beam is then periodically focused through a quadrupole-einzel-quadrupole lens set. It is collimated and then passed through a crossed electric magnetic field region, the Wien filter, for mass selection and is refocused into the interaction region by another quadrupole-einzel-quadrupole lens set. The focal spot in the interaction region is typically an ellipse of 1-mm^2 area with a convergence angle of about $f/15$. Under these circumstances, there are roughly 100 negative ions in the interaction volume at any one time.

The Wien filter may be set to zero resolution for simultaneous photodetachment of all beam components, or set to transmit a single mass, or switched rapidly among up to four different masses. Thus the difference measurements required for the use of Eq. (8) are made on a time scale which is short with respect to possible changes in contact potential due to surface chemistry in the interaction chamber. Overlapping photoelectron energy peaks due to different masses (particularly isotopes) may be independently stored and resolved in this way.

C. Laser

In the interaction region the ion beam is crossed perpendicularly by the intracavity photon beam of an argon ion laser (see Fig. 3). Littrow prism and Brewster-angle window optics produce a linearly polarized monochromatic laser beam. A low-loss half-wave plate inside the cavity allows us to rotate the polarization in the interaction region. A planoconvex lens of 25-cm focal length inside the cavity focuses the laser beam to a 0.1-mm-diam spot, yielding a 200–500-kW/cm^2 photon flux in the interaction region. The beam is refocused back through the interaction region by a 31.7-cm-radius mirror mounted inside the vacuum tank. Precision three-axis translation of the lens is provided. As the laser spot is small compared to the ion-beam size and is translatable, we can optimize the photoelectron source position for the electron energy analyzer. The laser is typically operated on the 4880-Å line, but several other lines, particularly 5145 Å, are usable when desired.

Although graphite, alumina-ceramic, and sectioned-tungsten laser discharge tubes were employed in various phases of the work, the present tubes are fabricated from fused silica. Because of the very high thermal loading of the 1-mm wall

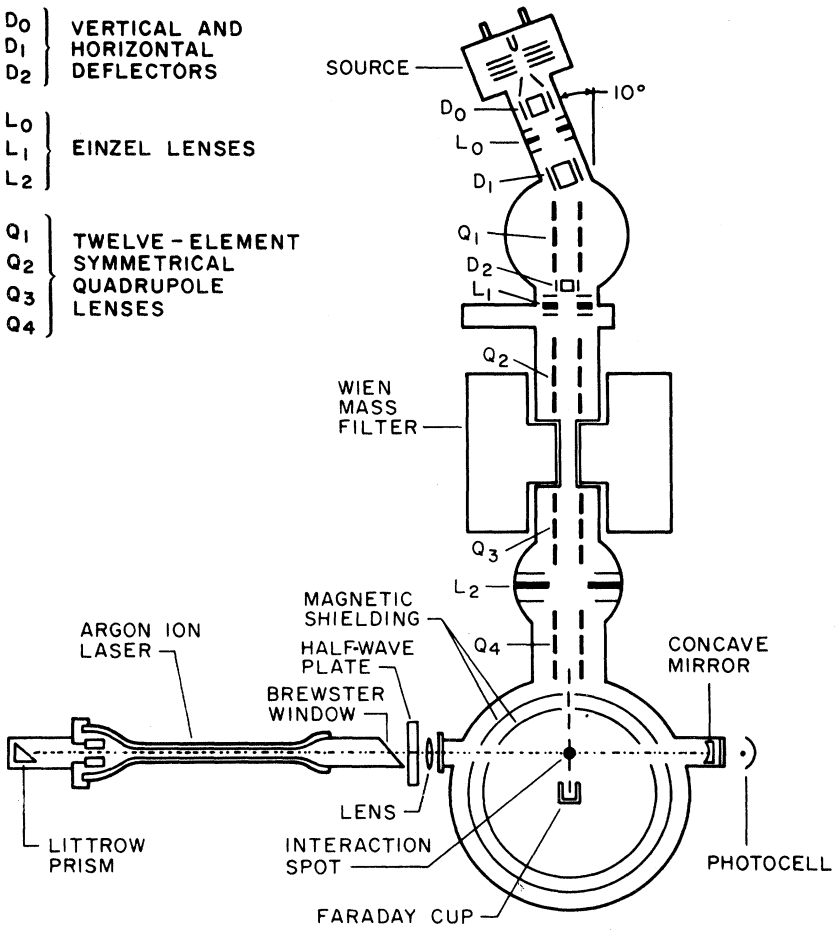

FIG. 3. Laser photodetachment photoelectron spectrometry apparatus in the crossed ion-beam–laser-beam configuration.

separating the argon plasma from the cooling water, the laser tube runs with a regrettably modest safety margin. The instantaneous laser output increases very rapidly—almost quadratically—with increasing discharge current. Therefore, by pulsing the discharge we can obtain a significant increase in time-averaged laser power at a fixed time-averaged thermal input, and hence fixed danger level. At the relatively high input powers involved (~6 kW), by far the most useful alternative is to operate the laser from the unfiltered, but full-wave rectified output of a suitable 60-Hz step-up transformer. Therefore, a duty factor of $\frac{1}{2}$ yields (ideally) a factor of 2 increase in the average data rate as compared to the continuous operation situation.

The laser discharge is initiated at the 120-Hz rate by a synchronized 30-kV positive pulse applied to a trigger wire wrapped outside the water-cooling jacket surrounding the actual laser capillary. The laser intensity and duty factors are controlled by changing the primary voltage applied to the transformer and by changing the series ballast resistor "dc" circuit between the rectifiers and the laser anode. The time-averaged discharge current is 12–15 A, which results in 20-50 circulating W of intracavity laser light in one line.

D. Electron Energy Analysis

Electrons photodetached into a $4\pi/2000$-sr solid angle perpendicular to the crossed ion–photon beams are accelerated by a variable acceleration lens, then a fixed acceleration lens, and injected into the hemispherical electron energy analyzer,[11] which operates at a fixed transmission energy of 11.2 eV (see Fig. 4). The variable acceleration is produced by applying +0 to +2.5 V to the interaction region, which is followed by a lens element at +2.5 V. The fixed acceleration occurs between the element at 2.5 V and analyzer input shield lens, held at 11.2 V. Thus an electron ejected into the acceptance cone with kinetic energy Ω eV will be accelerated to the transmission energy only when the interaction region is at Ω eV. The aperture which defines the angular acceptance is located in a field-free area within the interaction region to ensure that the angular acceptance is constant as a function of energy. The theoretical full

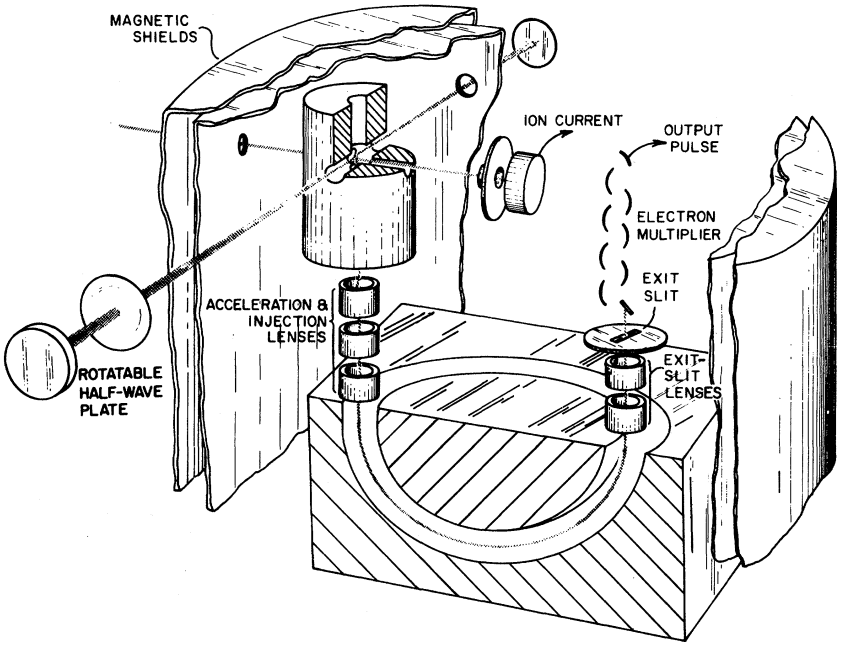

FIG. 4. Interaction chamber including the hemispherical electron monochromator.

width at the $1/e$ height for our analyzer geometry and working voltage is 40 meV.

The output end of the energy analyzer consists of a lens system for acceleration to 112 V, an exit slit, and a high-gain low-noise particle multiplier. Multiplier output counts are recorded as a function of instantaneous voltage on the interaction chamber, thus giving us number of electrons vs electron energy. The ion-beam current is collected by a shielded Faraday cup located beyond the interaction region, and the current is monitored by a Keithley model No. 601 electrometer or by a fast logarithmic amplifier.

The interaction region is made of carefully machined vacuum-fired graphite, a material which we have found to be superior to oxygen-free high-conductivity (OFHC) copper and gold plate in its stability against contact potential changes with beam constitution. The input optics, hemispherical analyzer, and exit optics are heavily gold-plated OFHC copper. The interaction region, lenses, analyzer, particle multiplier, and Faraday cup are enclosed in two Permalloy[20] magnetic shielding cans, with appropriately located small holes for the ion and photon beams. After suitable shield demagnetization the residual internal field is of the order of 1 mG.

E. Timing and Logic

The experiments are carefully timed to accurately maintain distinct signal (laser-on) and background (laser-off) channels. The background is sufficiently monotonic and photodetachment peaks sufficiently intense that the background measurement is not really necessary to the affinity determination. However, it is essential to the angular distribution measurement that an isotropic component of the distribution be distinguished from the background level.

Alternate zero crossings of the power-line voltage initiate a new laser-on–laser-off cycle. Start and stop commands, both manual and automatic, are logically gated to ensure that all data runs contain an integral number of complete laser-on–laser-off cycles. The background and signal periods, and the laser triggering pulse, are derived by appropriately counting pulses from a 100-kHz crystal clock. Built-in dead times, during which neither signal nor background counts are stored, protect against the possibility of a weak laser discharge continuing into the background segment.

Two analyzer sweeping techniques have been employed. Most of the NO^- data were collected using the first technique, and most of the O_2^- data using the second technique. Appropriate checks show that the two methods produce the same results.

In the first analyzer sweeping mode, an ultralinear ramp voltage, whose minimum, maximum, and slope may be set, is applied to the interaction chamber. A photodetached electron is transmitted by the electron analyzer if its initial kinetic energy divided by charge is equal to the voltage on the interaction chamber. Each particle multiplier count initiates sampling of the sweep voltage, and storage of one count in the multichannel analyzer channel corresponding to the instantaneous

voltage, i.e., the sampled voltage analysis mode. The count is stored in the first or second half of the analyzer memory, depending on whether it arrived during the time the laser was on or when the laser was off.

Photodetachment spectra can be collected for either the full beam, or for one ion mass component. The full beam is used to record simultaneously photodetachment from the desired species and the reference ion (O^- in both the NO^- and O_2^- experiments). The disadvantages of this method are that peaks corresponding to different mass ions may overlap, and time may be wasted sweeping through regions where no peaks of interest occur. Selecting a single mass is useful in studying its photodetachment spectrum for comparing peak intensities and spacing corresponding to various transitions, and for determining angular distributions corresponding to a single peak.

In the second analyzer sweeping mode, the multichannel analyzer is stepped through one channel at a time by a precision clock, i.e., the multichannel scaling mode. The 1024 channels are addressed in groups of 128 channels, providing eight analyzer blocks for storage, consisting of a signal block and a background block for each of the four masses. Each signal and background block pair is provided with an independent offset voltage. A digitally stepped voltage proportional to the instantaneous channel number is added to this offset, and the total voltage determines the transmission energy of the electron analyzer. Each particle multiplier pulse causes one count to be stored in the appropriate channel. Dwells of from zero to nine laser-on–laser-off cycles of $\frac{1}{120}$ sec each can be chosen for each signal and background block pair. As the programmer switches through the blocks, it simultaneously switches the electric field of the Wien filter to values corresponding to the selected masses. Thus we can select portions of the photedetachment spectra of one to four masses for simultaneous recording. Since we have the option of transmitting the same mass in more than one block, we can simultaneously record widely separated peaks belonging to the same mass, without wasting time looking at the region between them. The voltage increment applied to the analyzer may be set to 1.00, 2.50, 5.00, 10.00, or 20.00 meV/channel in order to change the number of channels into which a peak is divided. Combining the errors in the offset voltages and the voltage increments gives a worst-case error of ±0.25 meV on the electron energy scales used in these experiments.

F. Peak Shapes

Each photodetachment peak is fit to a slightly asymmetrized Gaussian form, providing the peak center c_0, baseline b, height h, half-width w, at $1/e$ height and asymmetry parameter a:

$$\mathfrak{N}(c) = b + h \exp\left[-\left(\frac{c-c_0}{w}\right)^2 - a(c-c_0)^3\right], \quad (11)$$

where $\mathfrak{N}$ is the total number of counts. Starting values for the five-parameter iterative least-squares fit[21] are chosen by the program, but the choice may be overridden by the user. We have investigated the effects of various starting values, of holding one parameter fixed, and of changing the range of channels considered by the program. In Fig. 5 we show the resulting changes in the residuals of the fit for a typical case in which individual parameters are fixed.

G. Angular Distributions: Technique

Angular distributions are recorded, as previously mentioned, one electron energy peak at a time. We set a precision power supply to provide the analyzer voltage corresponding to the peak of interest. A motor-rotated half-wave plate, gear coupled to a stopless potentiometer, is continuously rotated (~0.1 rev/sec), rotating the polarization through 4π rad per revolution of the plate. Each electron count initiates sampling of the potentiometer voltage and storage of a count in the appropriate channel of the signal or background multichannel analyzer block. A position-activated switch on the half-wave-plate mechanism provides delays for the manual start and stop commands, to ensure that every data run contains an integral number of complete rotations.

Since laser optical-system losses change slightly as the half-wave plate is rotated, the raw angular distributions must be normalized by the laser intensity as a function of half-wave-plate position. Thus during one revolution out of ten, the multichannel analyzer is automatically switched to a third block, and the laser intensity converted to a pulse rate by a photocell–electrometer–voltage-to-frequency–converter chain. These pulses initiate sampling of the potentiometer voltage, thus recording the laser intensity as a function of half-wave-plate angle. More recently the logic has been improved to allow recording of the product of the ion-beam current and the laser power in the intervals between photodetachment signal counts.

H. Angular Distributions: Data Reduction

After subtracting the background and normalizing the data by the laser intensity, we fit each angular distribution set by the nonlinear-least-squares program[21] to a sum of the first six Legendre polynomials, which are functions of $\cos\theta$, where θ is the polarization angle. When it has been determined that there are no significant amplitudes of order higher than $P_2(\cos\theta)$, which could indicate higher than dipole terms in the theory, the data are fit to

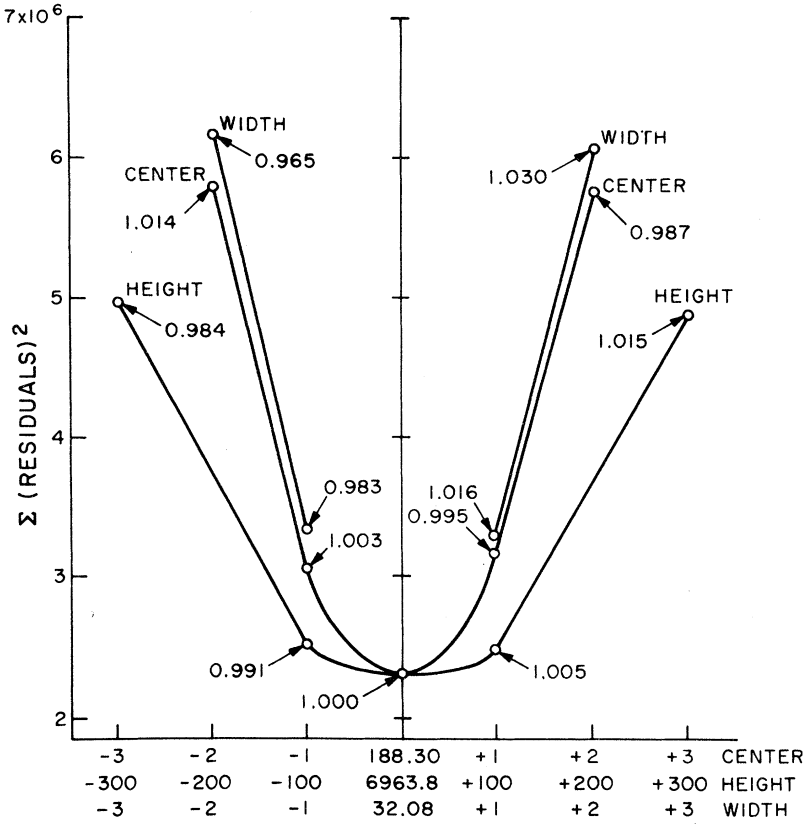

FIG. 5. Residuals of the five parameter least-squares fit to the peak shapes, as a function of various parameters being moved away from their optima. On the abcissa the units of center and width are channels (1.19 meV/channel) and the units of height are counts. At each point the relative peak area is also indicated.

a function of the form

$$I(\theta) = F[1 + G\,\sin(\tfrac{1}{2}\theta + \delta)][1 + \beta P_2(\cos\theta)]. \qquad (12)$$

In Eq. (12), the last bracket is the theoretically predicted relationship.[13] The first bracket is included to allow for a systematic variation in the ion-beam–laser-beam spatial overlap, caused by the rotation of the half-wave plate. Since the polarization vector rotates through 4π rad for each 2π-rad rotation of the half-wave plate, the systematic modulation caused by the changing spatial overlap will be at half the frequency of the angular distribution, and will not affect the value of β determined by the fitting program. The value of G was always negligibly small in these experiments, and the experimental angular distributions are almost entirely of the form $1 + \beta P_2(\cos\theta)$.

If the angular distribution reaches its maximum perpendicular to the polarization (as is the case for both NO^- and O_2^-), and a photodetachment energy peak has been measured at its angular maximum, then the total cross section for the transition $NO(v', v'')NO^-$, which we denote $\sigma(v', v'')$, is given in terms of the area under the corresponding photodetachment electron energy peak, $A(v', v'')$, by

$$\sigma(v', v'') \propto A(v', v'')/(1 - \tfrac{1}{2}\beta). \qquad (13)$$

Equation (13) is derived by evaluation of Eq. (9) at $\theta = 90°$.

A small kinematic rotation of the angular distribution in the lab frame occurs, since electrons ejected at a given angle to the crossed ion and photon beams in the center-of-mass frame have an additional velocity component (equal to the ion-beam velocity) in the lab frame. Even for one species of ion, angular distributions corresponding to different photodetachment peaks are rotated differently, since the relevant angle χ is $\tan^{-1}(U_{\text{beam}}/V_L)$. The kinematic rotation appears as a phase shift in the angular distribution, and this phase shift is a parameter in the fitting program. As a check, we require the program to yield the theoretical rotation angle within mechanical uncertainties.

J. Franck-Condon-Factor Fits

Once the labeling of transitions corresponding to the photodetachment peaks has been established, as discussed below, trial values of negative-ion molecular constants ω_e'' and r_e'' are assumed. They are then varied until calculated Franck-Condon factors approach a best fit to the observed relative photodetachment cross sections. The final fit is accomplished using the neutral molecule potential generated by the program RKR,[22] and the negative-

ion potential calculated from a Morse plus centrifugal potential by the program MORSE.[22] These programs generate a numerical internuclear potential defined by the input spectroscopic constants. Franck-Condon factors are then obtained using the program FCF,[22] which finds numerical solutions to the Schrödinger equation with the above potential, and computes the appropriate overlap integrals. Preliminary estimates and reasonableness checks were made with a considerably less-sophisticated program, which algebraically generated eigenfunctions of the Morse potentials[23,24] for the molecular and assumed ion states, and calculated the appropriate overlap integrals.[25] The use of the longer more-sophisticated programs in the final analysis was dictated by the low statistical uncertainty in the experimental results, i.e., changes of ω_e'' by 1% and r_e'' by 0.001 Å had a marked effect on the sum of the squares of the residuals of the fit.

IV. CHECKS AND CALIBRATIONS OF APPARATUS

We must investigate carefully the possible existence of various mechanical, electronic, and other instrumental effects which, if undetected and uncorrected, could lead to serious errors in our results.

A. Mechanical Collection Angle

If the electron-collection angle with respect to the crossed ion and photon beam is not precisely centered on 90° (see Fig. 1), then the term

$$2[(m/M)\,W\Omega]^{1/2}\sin\phi \tag{14}$$

in Eq. (6) is a nonzero function of the outgoing electron energy. For typical data discussed here and in the following paper, this term could introduce an error of as much as 1 meV/deg in an affinity difference measurement if the uncorrected form of Eq. (8) were used.

However, we have a sensitive check for the presence of such an error: We can simultaneously photodetach H^- and D^-, two light species with a large (1:2) mass ratio, a situation which maximizes kinematic effects. Since for this application there is a negligible difference in the electron affinities of H and D, Eq. (6) provides the misalignment angle

$$\phi_m = \sin^{-1}\frac{(\Omega_D-\Omega_H)+mW(1/M_D-1/M_H)}{2(mW)^{1/2}[(\Omega_D/M_D)^{1/2}-(\Omega_H/M_H)^{1/2}]}\,. \tag{15}$$

The simultaneous photodetachment of H^- and D^- has been done recently in our apparatus, and we place an upper limit of 0.02 rad on the misalignment angle, leading to a shift of less than 0.6 meV in the affinity of NO.

B. Calibration of Electron Energy Analyzer

We must consider the possibility of a mechanical problem in the electron energy analyzer (real or virtual slit in the wrong place, nonspherical "hemispheres," etc.) or a failure of the electron injection optics. Two possible consequences are a differential effect, in which the measured spacing between two peaks does not correspond to their correct spacing, and a transmission effect, in which the ratio of two peak areas normalized by their angular distribution constants as in Eq. (13) does not correspond to their relative cross sections.

Great care has been taken in the design of the electron energy analyzer system to ensure that its transmission is constant as a function of transmission energy. This is relatively easy to accomplish because the data used do not span a large dynamical energy range. The form in which we state our relative cross sections, i.e., as the ratios of properly normalized intensities of adjacent peaks, minimized the severity of any transmission error on our results. We will show later that even very pessimistic assumptions about variation of transmission with transmission energy do not significantly affect our results.

We became aware of an energy differential effect when the observed spacing between NO^- photodetachment peaks was found to be about 3% less than the spectroscopic spacing of the NO vibrational levels, with a small systematic variation as a function of absolute electron energy. This effect was at first informally discussed[25] as being attributable to a strong dependence of Franck-Condon factors on initial ion rotational state, leading to different non-Maxwellian rotational distributions in each final neutral vibrational state. Subsequent calculations showed that the calculated effect is 10 to 100 times too weak to account for the observed small spacings. Further cause for suspicion of a systematic effect arose when the O_2^- data were collected, and showed the same 3% too-small spacing between peaks.[26]

A demonstration of the presence of an energy-scale compression in our electron analyzer is available from the O_2^- data.[7] Briefly stated, we observe photodetachment from a single O_2^- vibrational state to both the $X\,^3\Sigma_g^-(v'=1)$ and $a\,^1\Delta_g(v'=1)$ states of neutral O_2. Since the energy difference between these two states is well known, it is possible to determine the energy-scale calibration factor accurately. The value obtained in this manner is (3.10 ± 0.05)%.

As another test, we use the recently developed wavelength tunable dye laser technique of Lineberger and Woodward[27] for observing atomic photodetachment thresholds to better than 0.5-meV pre-

cision. They have extended the experimental value for the electron affinity of atomic sulfur to four significant figures. Using the value of Branscomb *et al.*[15] for the electron affinity of atomic oxygen as another standard we calculate from Eq. (8) the difference in electron energy of electrons simultaneously photodetached from S^- and O^-. The energy difference we measure is $(3.0 \pm 0.5)\%$ smaller than the correct value.

Each of the above two tests measures an average correction over a fairly large range, while comparison of each measured vibrational splitting with its spectroscopic value gives a local determination. When all of the tests are considered, the correction factor is determined to be $(3 \pm 0.5)\%$.

Measurements on four different photodetachment systems, $S^- - O^-$, $X\,^3\Sigma_g^- - a\,^1\Delta_g O_2$, and the vibrational spacings in NO^- and O_2^- photodetachment, each produced an approximately 3% correction factor. We conclude that the 3% average compression describes an aberration of our electron energy analyzer.

V. NO^- PHOTODETACHMENT DATA

A. Complete Electron Spectrum

In Fig. 6(a), we show the electron energy spectrum obtained when the entire ion beam, composed mostly of NO^-, O_2^-, and O^-, is crossed with 4880-Å photons. Here the Wien filter is set to zero resolution. The NO^- peaks are labeled by the transition to which they will be shown to correspond. The O_2^- spectrum and the O^- photodetachment peak are also so labeled.

Figure 6(b) shows the photodetachment spectrum obtained with the Wien filter adjusted to transmit only mass 30, and the laser polarization adjusted to be approximately perpendicular to the electron-collection direction, corresponding to the maximum in the angular distribution. Figure 6(c) is also for NO^-, but with the photon polarization set along the direction of electron collection, corresponding to the minimum in the angular distribution. Note that the relative intensities of the peaks change from Fig. 6(b) to 6(c); this is primarily a consequence of the dependence of the angular distribution on outgoing electron energy for fixed electronic states.

The data presented in Figs. 6(a)–6(c) are qualitatively useful, but are not used as the basis for any precise measurements: They provide an overall view of the observed quantities, but with less than the maximum attainable accuracy.

B. Adjacent Peaks in Energy Spectrum

Figure 7 shows data for two electron energy peaks, corresponding to $NO(3,0)NO^-$ and $NO(2,0)NO^-$, where the polarization was such as to maximize the counting rate. The energy scale is 1.25 meV/channel in this case. The smooth curve is a weakly skewed Gaussian least-squares fitted to the data [see Eq. (11)]. From the fitted curves we obtain precise peak separations and the areas under each peak.

We have accumulated similar data sets for all adjacent peak pairs shown in Figs. 6(b) and 6(c) except the $NO(6,0)NO^-$ transition, whose signal was too small to allow us to obtain good statistics within a reasonable integration time. The statistical scatter of data points about the fitted curve shown in Fig. 7 is quite typical: The less intense peaks were collected over longer times, yielding roughly the same signal-to-noise ratios.

C. Measurement of Absolute E_{vd}^T $(NO(3,0)NO^-)$

To determine the zero of the electron energy scale independent of contact potential differences, we simultaneously measure electron energies of one of the $NO \leftarrow NO^-$ transitions and of the $O \leftarrow O^-$ transition. In Fig. 8, we show, as an example, two electron energy peaks that are due to photodetachment from O^- and the $NO(3,0)NO^-$ transition. These data are obtained by programming the ion mass filter to alternate rapidly between transmitting O^- and NO^-, and simultaneously to alternate the electron energy analyzer between the two regions of interest, and appropriately route the corresponding photodetachment signals.

D. Angular Distribution Data

Figures 9(a) and 9(b) illustrate the photodetachment angular distribution data for $NO(2,0)NO^-$ and its reduction. Figure 9(a) shows the raw photodetachment signal, the background noise signal, and the laser power as a function of angle. Figure 9(b) shows the normalized data and the least-squares-fitted function. Similar data sets exist for the other transitions. The range of angle, approximately 4π, corresponds to one mechanical rotation of the half-wave plate, two rotations of the polarization, or four repetitions of the fundamental angular distribution.

E. Isotopic Data

Using the same mass switching technique described above, we measured simultaneously vertical detachment energies corresponding to the two isotopes NO^{16-} and NO^{18-}. The specific transitions observed were $NO^{18}(0,0)NO^{18-}$, $NO^{18}(1,0)NO^{18-}$, $NO^{16}(0,0)NO^{16-}$, and $NO^{16}(1,0)NO^{16-}$. Figure 10 presents these data. Table I lists all of the relevant numbers obtained from these and similar data as provided by the curve fits and initial reduction.

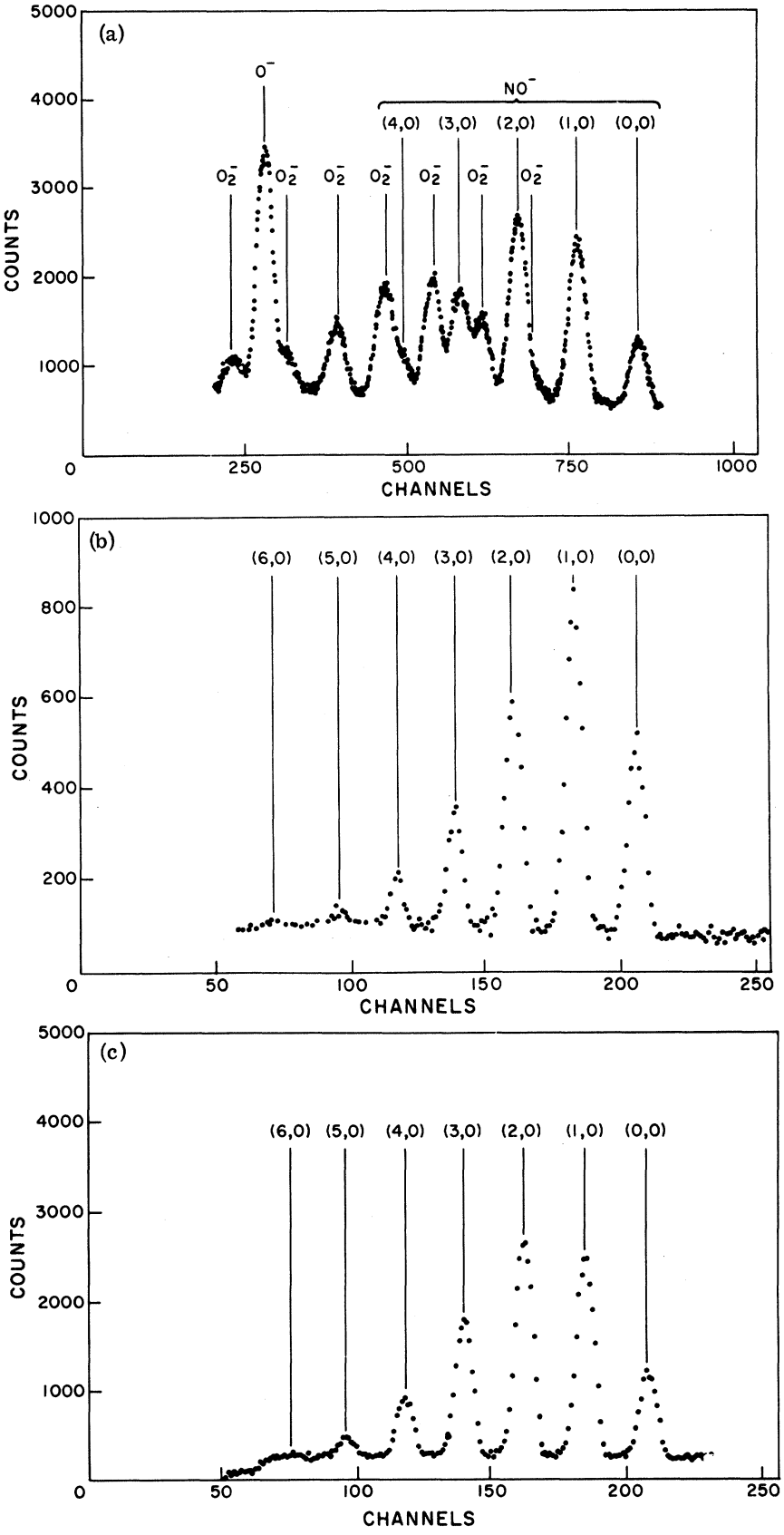

FIG. 6. Photodetachment spectra. (a) Simultaneous photodetachment of the entire beam showing the O^- and O_2^- peaks, and the NO^- peaks which are labeled by the transitions to which they belong. The x scale is 2.50 eV/1024 channels. (b) The beam is mass selected for NO^- and the spectrum is taken for polarization perpendicular to electron collection. (c) NO^- with polarization parallel to electron collection. The abscissa is 2.5 eV/257 channels.

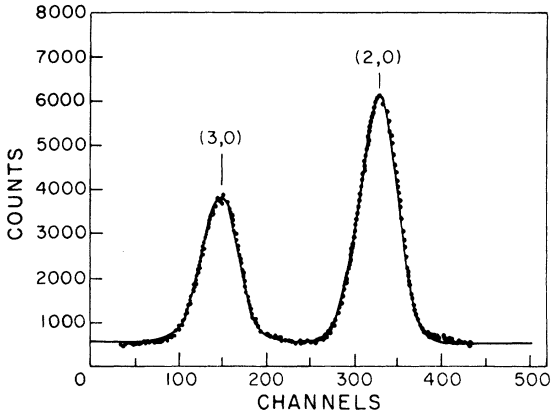

FIG. 7. Example of the data yielding peak spacing and intensities, showing the NO(3,0)NO⁻ and NO(2,0)NO⁻ peaks and their fits by the five-parameter iterative least-squares program. The abscissa is 0.625 eV/512 channels, or 1.19 meV per point.

VI. IDENTIFICATION OF INITIAL AND FINAL STATES

A. Demonstration of Single Initial Vibrational State

Inspection of the data [Fig. 6(c)] clearly shows that the NO^- photodetachment spectrum is a single series of almost equally spaced peaks. Thus there is either a single initial vibrational state and multiple final vibrational states, or a single final vibrational state and multiple initial vibrational states. By prolonged signal integration between peaks, and by running the source under a wide range of pressures and discharge currents, we have confirmed that multiple interwoven series, which would correspond to multiple initial and final states, never appear.

Since the peak spacing smoothly decreases with decreasing electron energy, this single series must correspond to multiple final vibrational states and a single initial vibrational state. Multiple initial and single final states would lead to peak spacing decreasing with increasing electron energy. This is an elementary consequence of the fact that molecular vibrational energy levels become more closely spaced as the vibrational quantum number increases.

B. Evidence for Initial-State Identification

1. Franck-Condon-Factor Envelope

The "Franck-Condon-factor envelope" of a molecular vibrational progression is a smooth curve connecting the points that represent individual Franck-Condon factors on a graph whose ordinate is transition intensity and whose abscissa is the final-state vibrational quantum number. It is recognized[28] that this envelope is single peaked in absorption only if the initial state is $v''=0$. If $v''>0$, the envelope has at least two maxima and at least one easily discernible minimum. Spectroscopic data and numerous numerical experiments confirm this point. This quite general principle is easily visualized by noting the variation predicted in the shape of intensity distributions when a Condon parabola is plotted on a Deslandres table. Only for progressions from $v''=0$ can a single intensity maximum occur. As a check of the applicability of this principle, calculations were made[22] of the Franck-Condon factors linking a particular lower vibrational state to the probression of upper vibrational states. A wide range of spectroscopic parameters were considered for the lower state. For any reasonable values of the Morse potential parameters only the $v''=0$ progression produced the required single-humped intensity envelope. No other progression or portion of a progression could be misinterpreted in such a way as to give the required result.

The form in which our data are received and displayed, i.e., Fig. 6, directly shows the shape of the Franck-Condon-factor envelope of the initial state. Clearly, this envelope has a single maximum. Detailed analysis, including the effect of varying angular distributions and the dependence of the electronic part of the cross section on outgoing electron energy, do not modify the single peakedness of the envelope. Thus we conclude that the single initial state is $NO^-(v''=0)$.

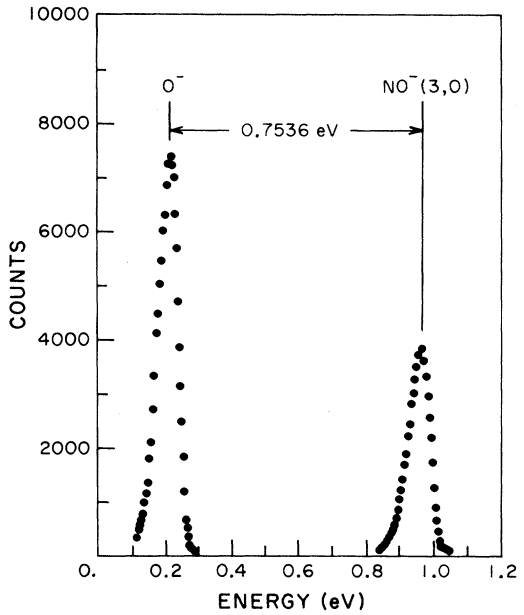

FIG. 8. The data yielding vertical detachment energies based on $EA(0)$. This figure shows the O^- and NO(3,0)NO^- peaks, as simultaneously collected and resolved by the technique of rapidly chopping between two masses and separately storing the corresponding spectra.

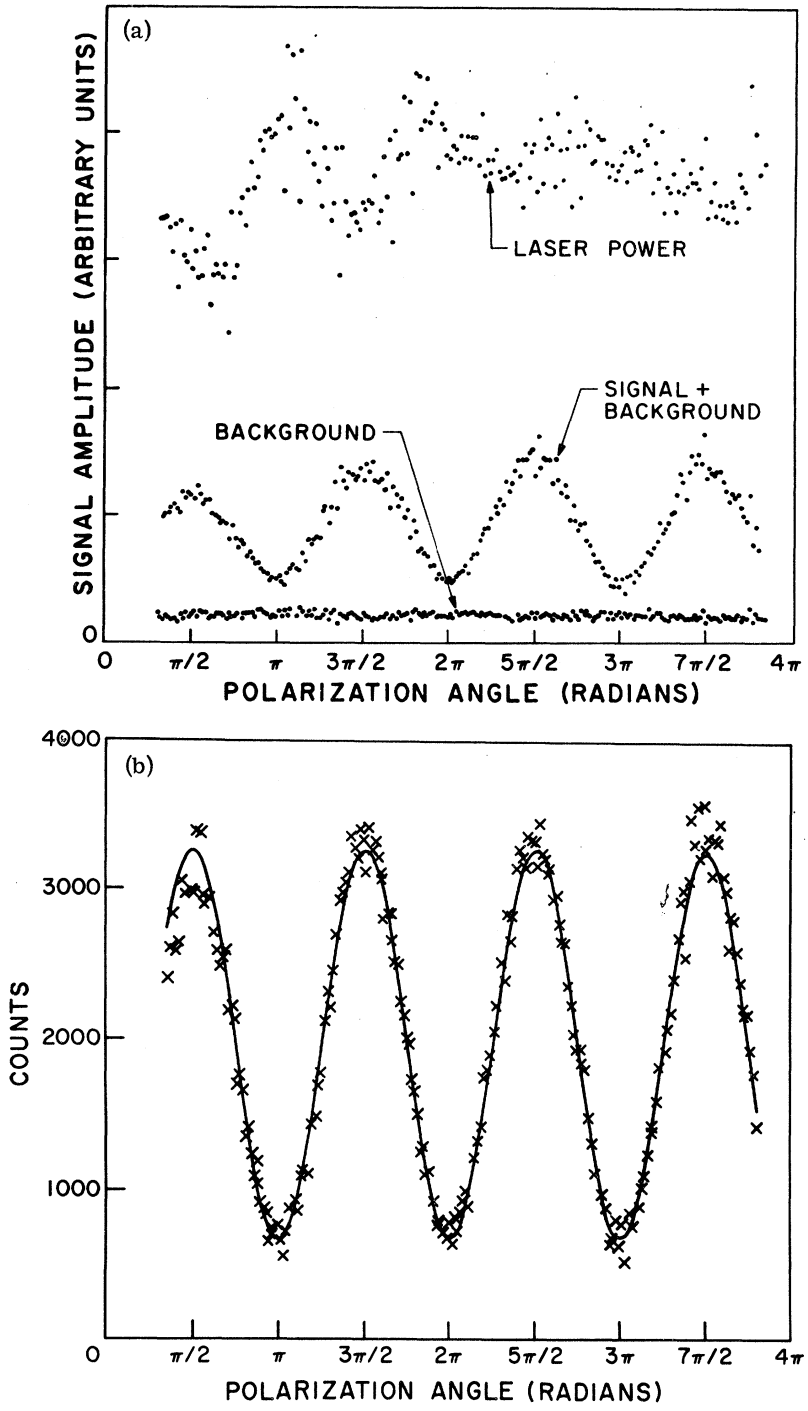

FIG. 9. Angular distribution data. (a) The signal plus background, background alone, and laser power as a function of half-wave-plate angle. (b) The corrected angular distribution and its fit with the form of Eq. (12).

2. Modification of Source Conditions

We have systematically changed the source gas pressure and discharge current in an attempt to produce an NO^- beam whose photodetachment spectrum is different from that shown in the various data-set figures. Under no circumstances have we observed a modified spectrum. Experience with this source, using both atomic (C^-)[12] and molecular (O_2^-)[7] negative ions indicates that pressure and discharge-current changes produce marked changes in the initial-state distribution, if such changes are possible.

We attribute our inability to produce different initial states to (i) the instability against autodetachment of vibrational states higher than the one we

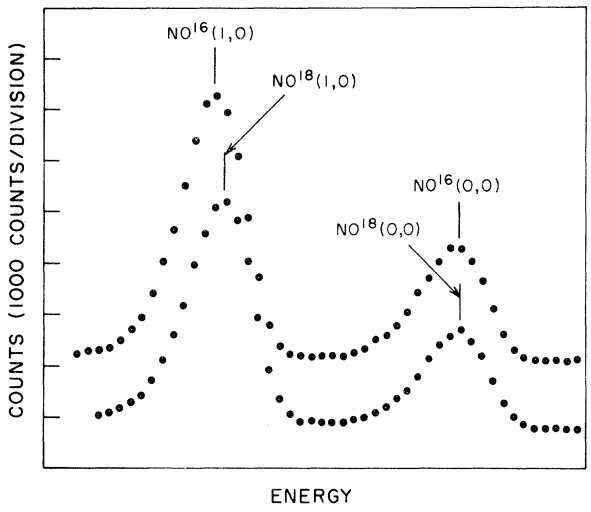

FIG. 10. Isotopic data used to identify the final vibrational-state assignment. Points along the abscissa are at 10-meV intervals.

observe and (ii) the nonexistence of vibrational states lower than the one we observe. Thus we again conclude that our NO^- beam is entirely in the $v''=0$ state.

C. Evidence for Final-State Identification

To determine unequivocally the final-state assignment for the transition we observe, we use three independent techniques: (i) peak spacing, (ii) Franck-Condon-factor envelope smoothness, and (iii) isotopic substitution. Each technique is subject to different systematic errors. An uncorrected error in the energy scale of our analyzer could cause an error in the state identification by method (i), but would not affect the result obtained by methods (ii) and (iii). An uncorrected transmission effect in the energy analyzer would affect only the result obtained by method (ii). Method (iii) is insensitive to either energy scale or transmission errors. Each method yields an unambiguous result, and each result agrees with the other two. We take this agreement as conclusive proof that we have identified correctly the observed final vibrational states, and also as evidence that any unidentified systematic errors are small.

1. Peak Spacing

Since the electron energy spectrum exhibits vibrational structure characteristic of the neutral NO molecule, and the anharmonicity of the NO vibrational energy levels is well known, careful measurements of the energy difference between adjacent peaks determine the final vibrational-state assignment. Since the anharmonicity is small ($\omega_e x_e \approx 0.01\,\omega_e$) a very precise measurement is necessary. Figure 11 shows the spectroscopically obtained value for the energy difference plotted with the experimental value and the associated error estimate. The error estimate is the sum of the ± 0.005 error in the 1.030 scale correction factor and the statistical errors originating in the determination of the centers of the two peaks in question. The two right-most data points are shown with dashed error bars because they do not fall in the calibrated range of our energy scale where the correction is known to be 1.03 ± 0.005.

2. Franck-Condon-Factor Intensity Envelope Smoothness

If the transition yielding the highest-energy electrons, i.e., the right-most transition in Fig. 6(c), were not the $NO(0,0)NO^-$ transition, but instead one where the final state had, for example, $v'=1$, then we would expect to see one more peak, higher in electron energy. Only if the Franck-Condon factor for the $NO(0,0)NO^-$ transition were below our noise level, would it be possible for us to overlook that transition. If the right-most transition of Fig. 6(c) were labeled as $NO(1,0)NO^-$, instead of $NO(0,0)NO^-$, then we would expect to find some evidence of the $NO(0,0)NO^-$ transition one NO neutral vibrational interval to the right. Figure 6(c) shows no evidence of such a transition. In addition, very long periods of signal integration

TABLE I. Summary of measured data.

Transition	Measured spacing (meV)	β	Peak	Relative area	Corrected relative area
(0,0)	235.1 ± 0.5	-0.626 ± 0.005	152 181	2.629	2.535
(1,0)			400 032		± 0.099
(1,0)	230.9 ± 0.5	-0.723 ± 0.005	268 532	1.049	1.016
(2,0)			281 823		± 0.036
(2,0)	226.4 ± 0.5	-0.813 ± 0.012	307 324	0.570	0.569
(3,0)			175 274		± 0.023
(3,0)	222.8 ± 0.7	-0.820 ± 0.009	241 524	0.365	0.359
(4,0)			88 132		± 0.019
(4,0)	217.5 ± 1.0	-0.867 ± 0.010	66 477	0.303	0.302
(5,0)		-0.87 ± 0.05	20 173		± 0.029

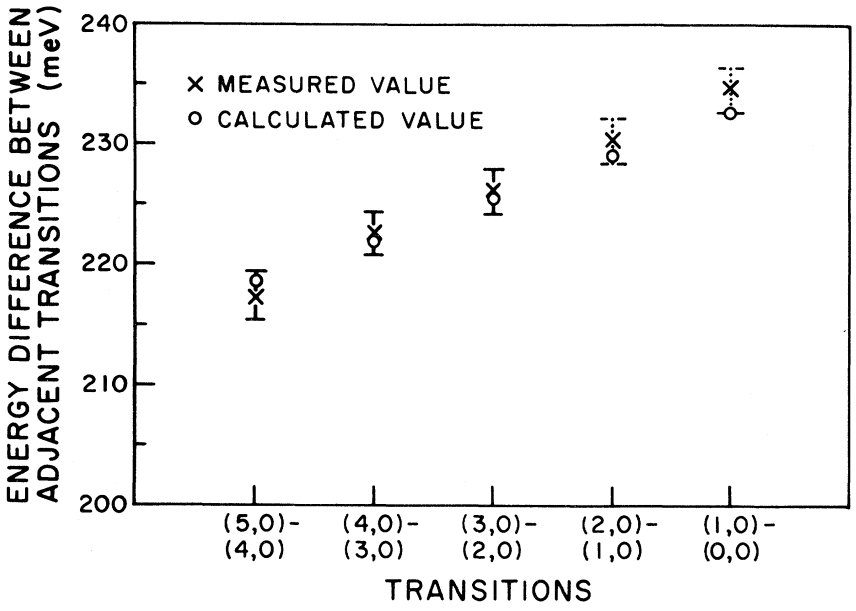

FIG. 11. Plot of the measured splittings (×) and their spectroscopic values (○) vs the transition they identify. The error bars represent the total error in the measurement.

in the energy range where an extra peak would occur confirms that no such peak exists.

The general smoothness required of Franck-Condon-factor intensity envelopes indicates that were an extra peak present, its intensity would be about 20% of the intensity of its left adjacent peak. Thus it would be easily visible. This is true for any upper-state assignment and any set of vibrational wave functions that yield reasonable fits to the observed peak intensities. The end of the spectrum occurs well before the falling off of the Franck-Condon-factor envelope has made additional transitions undetectable. This requires that the highest electron energy peak observed belong to a final state with $v' = 0$. Thus we assign the right-most transition in Fig. 6(c) to NO(0, 0) NO^-, and the other transitions, in the direction of decreasing electron energy, to NO(1-6, 0)NO^-.

3. *Isotopic Evidence*

The third independent technique used in the final-state identification involves the use of an isotope of the ion under study and a measurement of the shifts caused in the observed spectra.

The classical expression for the vibrational frequency ν is

$$\nu = (1/2\pi)(k/\mu)^{1/2}, \tag{16}$$

where k is the force constant and μ is the reduced mass of the molecule. For isotopes (at our level of precision) the force constant k is the same, since it depends only on the electronic motion, and therefore the fundamental frequency ν is inversely proportional to $\mu^{1/2}$. It can be shown that, to a very good approximation,[29]

$$\omega_e^i = \rho\omega_e \text{ and } \omega_e x_e^i = \rho^2 \omega_e x_e, \tag{17}$$

where the superscript i refers to the isotope and $\rho \equiv (\mu/\mu^i)^{1/2}$. The isotope NO^{18} was used, so the vibrational frequency and the anharmonicity were reduced by 2.6 and 5.2%, respectively.

If we apply the isotope correction, neglecting the insignificant correction to $\omega_e y_e$ and the rotational terms, we find that the difference in vertical detachment energies, for the same transition but different isotopes, is

$$E_{vd} - E^i_{vd} = (1-\rho)\,\omega_e'(v'+\tfrac{1}{2}) - (1-\rho^2)\omega_e x_e'(v'+\tfrac{1}{2})^2 - [(1-\rho)\omega_e''(v''+\tfrac{1}{2}) - (1-\rho^2)\,\omega_e x_e''(v''+\tfrac{1}{2})^2]. \tag{18}$$

The difference $(E_{vd} - E^i_{vd})$ is much smaller than the separation between peaks; in fact, it is small compared to the peak width. Thus, the mass switching programmer is used in the isotope experiments, as described in Sec. III E. Since the shifts are small, there is no difficulty in determining which peaks in the two spectra belong to the same initial and final vibrational quantum numbers.

Since we have demonstrated that the initial state is the ground vibrational state, Eq. (18) reduces to

$$E_{vd} - E^i_{vd} = (1-\rho)\,\omega_e'(v'+\tfrac{1}{2}) - (1-\rho)\,\omega_e x_e'(v'+\tfrac{1}{2})^2 - [(1-\rho)\,\tfrac{1}{2}\omega_e'' - (1-\rho^2)\,(\tfrac{1}{4}\omega_e x_e'')]. \tag{19}$$

In this equation ω_e' and $\omega_e x_e'$ are known very precisely from infrared absorption spectroscopy, ω_e'' and $\omega_e x_e''$ can be taken from our results or from an independent determination,[30] and ρ is easily evaluated. Hence, a measurement of the dif-

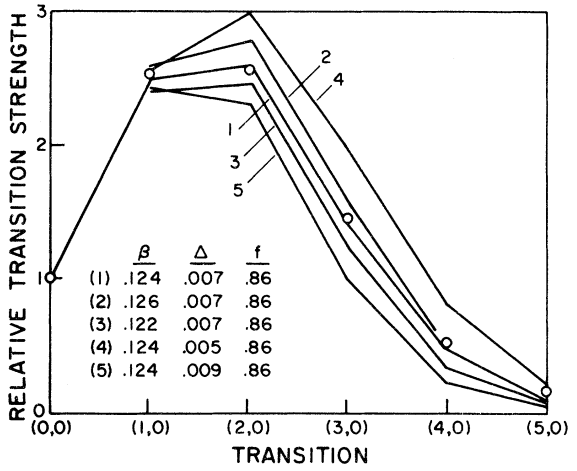

FIG. 12. Franck-Condon-factor fits to the observed intensities in the harmonic-oscillator wave-function approximation. The circles are the experimental intensities and the lines connect the calculated intensities. All intensities are expressed relative to the (0, 0) intensity; β and Δ are in Å.

ference in vertical detachment energies for the two isotopes determines, with the use of Eq. (19), the final vibrational quantum number v'.

The results of the isotope experiments were quite unambiguous. For the transition labeled NO(0, 0)-NO^- the value of v' calculated using Eq. (19) was 0.05 ± 0.17 and for the transition labeled NO(1, 0)-NO^- it was 1.06 ± 0.16. Figure 10 shows the raw isotopic data used in this determination.

Hence, it has been demonstrated in three independent ways that the final-state identification is correct. We conclude that the peaks we observe correspond to the progression NO($v' = 0-6$, 0)-NO^-, where the transition with $v' = 0$ corresponds to the right-most peak in Fig. 6(c).

VII. NO MOLECULAR CONSTANTS

A. Theoretical Basis

A complete description of the NO($X\,^2\Pi_{3/2,\,1/2}$) states in terms of spectroscopic constants is available.[31] For the negative ion we have our photodetachment data, which are, in part, experimental Franck-Condon factors connecting the NO^- electronic and vibrational ground state with the NO($X\,^2\Pi_{3/2,\,1/2}$, $v' = 0-6$) states. Thus it is attractive to parametrize the NO^- vibrational wave functions by the usual spectroscopic constants, then determine values of these constants which generate wave functions yielding best Franck-Condon-factor fits to the photodetachment intensity data.

1. Method

As a demonstration let us try to fit the experimental transition intensity ratios by Franck-Condon factors calculated between upper (NO) and lower (NO^-) vibrational states in the harmonic-oscillator approximation. In Fig. 12, we display the results of varying r_e'' and ω_e'' to obtain a good fit. The circles mark the data [intensities are normalized to the NO(0, 0)NO^- peak], and the smooth curves join the Franck-Condon factors for several values of $\beta \equiv r_e'' - r_e'$ and $f \equiv \omega_e''/\omega_e'$. Figure 12 actually contains a small increment in β, $\Delta = 0.007$ Å, for each NO vibrational level, as a first step toward putting in the anharmonicity of the NO levels.

We very quickly decide that this simple picture takes us most of the way toward fitting the data, and conclude that the method is going to provide surprisingly unique values of the parameters. Thus we are encouraged to seek a more complete description, in which our knowledge of the NO internuclear potential is more fully utilized.

2. Assumptions

We assume that photodetachment occurs on a time scale which is short with respect to molecular vibration and rotation times, so that the nuclear position and momenta cannot change appreciably during photodetachment. If correct, this assumption leads to the applicability of the Franck-Condon principle, i.e., the relative cross sections between various pairs of vibrational states belonging to two electronic states are largely determined by the squared overlap integral of the vibrational wave functions alone. Discussion of the vibrational wave function as a separate entity is of course based on the Born-Oppenheimer approximation. We expect that the rotational transitions present are the P, Q, and R branches characteristic of $\Pi - \Sigma$ transitions.

We make our measurements in an energy range 1.4–2.5 eV above threshold and shall assume that over this range the electronic matrix element is, to a good approximation, constant. As an experimental confirmation, we see no change in the photodetachment signal intensity when the photon energy is changed by 5% (4880–5145 Å). Any variation of the electronic matrix element with energy would have the same effect on our results as an electron energy analyzer transmission function which is a function of transmission energy. We shall see later that even very pessimistic assumptions about the severity of combined transmission and electronic cross-section effects modify our results very little.

B. Procedure and Results

1. Upper- (NO) *State Wave Functions*

The molecular constants of NO($X\,^2\Pi_{3/2,1/2}$) are known spectroscopically to an accuracy several

orders of magnitude greater than we need in the context of our Franck-Condon-factor fits to photodetachment intensities. Furthermore, our electron energy analysis cannot resolve the 14.9-meV spin-orbit splitting in the NO ground state.

Thus we use as upper-state wave functions numerical solutions to the Schrödinger equation with a Morse potential parametrized by the average of the spectroscopic constants[31]:

$$\omega_e'(\mathrm{NO}\,^2\Pi_{3/2,1/2}) = 1904.104\ \mathrm{cm}^{-1} = 236.08\ \mathrm{meV},$$

$$\omega_e x_e'(\mathrm{NO}\,^2\Pi_{3/2,1/2}) = 14.087\ \mathrm{cm}^{-1} = 1.746\ \mathrm{meV},$$

$$r_e'(\mathrm{NO}\,^2\Pi_{3/2,1/2}) = 1.15079\ \text{Å}\ .$$

Note that unlike the atomic multiplet case, the $\Omega = \frac{3}{2}$ and $\frac{1}{2}$ levels are equally weighted. The centrifugal potential added uses

$$B_e'(\mathrm{NO}\,^2\Pi_{3/2,1/2}) = 1.705\ \mathrm{cm}^{-1} = 0.211\ \mathrm{meV}.$$

The eigenfunctions of this total potential are generated by the program FCF,[22] as discussed in Sec. III.

2. *Starting Values for* NO^- *Molecular Constants*

There is a great deal of evidence to guide us to the proper starting values for ω_e'' and r_e'' in our fitting procedure. We note that the added electron in NO^- is antibonding and therefore $r_e'' > r_e'$. Gilmore[32] estimates $\Delta r_e = 0.05$ Å, and application of Badger's rule[33] would provide an estimate for ω_e''. Spence and Schulz[30] have used the trapped-electron method to measure $\omega_e'' = 170$ meV, and using Badger's rule they conclude that $r_e'' = 1.286$ Å.

Our preliminary Franck-Condon-factor fits, using harmonic-oscillator functions and the analytic overlap integral forms of Hutchisson,[34] indicate that $r_e'' \approx 1.27$ Å and $\omega_e'' \approx 200$ meV.

The molecular constants $\omega_e x_e''$ and B_e'' are not free parameters in the Morse-potential approximation. The dissociation energy D_e of a molecule described by a Morse potential is[23]

$$D_e = \omega_e^2/4\omega_e x_e\ . \tag{20}$$

Since the separate structure of NO^- is presumed to be $N + O^-$, we have

$$D_0(\mathrm{NO}^-) = D_0(\mathrm{NO}) - E_A(\mathrm{O}) + E_A(\mathrm{NO})\ . \tag{21}$$

Hence, using our nominal value for the electron affinity of NO, Eqs. (19) and (20) provide an estimate of $\omega_e x_e''$. The value of $\omega_e x_e''$ calculated by this procedure is probably too small, since Morse-potential representations generally predict too small a value for the dissociation energy. Fortunately, our fitting procedure is not very sensitive to small changes in $\omega_e x_e''$.

Alternatively, we can use the Spence and Schulz[30] value of 1.00 ± 0.25 meV for $\omega_e x_e''$. To maximize the accuracy of the final result, we adopt this alternative. Still we emphasize that the photodetachment analysis does not require this external input because it depends weakly on $\omega_e x_e''$.

Since the value of B_e is given by[35]

$$B_e = h/8\pi^2 c\mu r_e^2\ , \tag{22}$$

where c is the velocity of light, h is Planck's constant, and μ is the reduced mass, it follows, with the assumption that the reduced mass of NO^- and NO are approximately the same, that

$$B_e'' = B_e'(r_e'/r_e'')^2\ . \tag{23}$$

Thus, the free parameters in our fitting procedure are ω_e'' and r_e''. We use 1.00 ± 0.25 meV for $\omega_e x_e''$ and the program calculates the appropriate value for B_e'' for each trial r_e''.

3. *Fitting Data*

We calculate the envelope of Franck-Condon factors for the transitions $\mathrm{NO}(v' = 0-5,\ J' = 12,\ v'' = 0,\ J'' = 12)\mathrm{NO}^-$ on a two-dimensional grid in the ω_e''-r_e'' plane in the region around the scattering values indicated by the harmonic-oscillator approximation. The value $J' = J'' = 12$ corresponds to the maximum of the (Maxwellian) rotational state distribution at our estimated source temperature of 630 °K. The Franck-Condon factors are relatively insensitive to this choice of J; envelopes falling within the experimental error bars can be obtained for reasonable values of J and the resulting values of ω_e'' and r_e'' are not significantly different.

Each intensity sample is weighted by the inverse of its statistical uncertainty (variance), and at each point on the grid the weighted sum square error of the Franck-Condon-factor fit is calculated. The grid point corresponding to the minimum fitting error is then taken as a new starting value, and the procedure is repeated with a finer ω_e''-r_e'' grid. The sensitivity of this technique is such that two or three iterations take us to a grid size of about 16 cm^{-1} in the ω_e'' coordinate and 0.001 Å in the r_e'' coordinate. Making the grid finer than this does not lead to any statistically significant improvement in the fit to the data.

There remains the possibility that we have found a locally optimum fit in the ω_e''-r_e'' plane, but the result so obtained is not unique. We have carefully investigated this possibility by systematically forcing rather large excursions of ω_e'' and r_e'', attempting to find another region of good Franck-Condon-factor fits. We find no such region.

We express both our data and the calculated Franck-Condon factors in the form

$$\sigma[\mathrm{NO}(v'+1, 0)\mathrm{NO}^-]/\sigma[\mathrm{NO}(v', 0)\mathrm{NO}^-]\ ,$$

to minimize the propagation of statistical and systematic errors. Figure 13 shows the data, and the

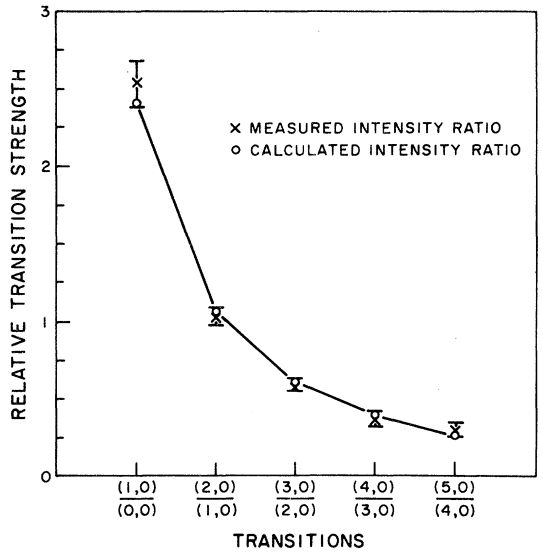

FIG. 13. Final Franck-Condon-factor fits, using the programs MORSE, RKR, and FCF and including the effect of rotation. Error bars are statistical (one standard deviation) and come from area measurements.

Franck-Condon-factor envelopes, for several values of ω_e'' and r_e''. We demonstrate the sensitivity of the technique by presenting the values of the parameters ω_e'', r_e'', and B_e'' which minimize the sum of the squares of the residuals. The error estimates indicate the sensitivity of the procedure and do not include, as yet, the possible systematic errors:

$$\omega_e'' = 1470 \pm 25 \text{ cm}^{-1}, \quad r_e'' = 1.258 \pm 0.001 \text{ Å},$$

$$B_e'' = 1.427 \pm 0.002 \text{ cm}^{-1}.$$

VIII. ELECTRON AFFINITY OF NO

A. Multiplicity of O^- Peak

Both the O^- and NO^- photodetachment peaks consist of multiple transitions which are too closely spaced to be resolved by our electron energy analyzer. We know the separations of the fine-structure components and can estimate the relative intensities of the transitions. We would like to convince ourselves that under these circumstances, given the resolution of our analyzer and typical fine-structure splittings, we could from a determination of the center of the resulting peak, determine with high accuracy the location of the fine-structure states.

To investigate this point, we generate an artificial data peak by summing two Gaussians, in the height ratio of 2:1, separated by 15 meV. The full widths at the $1/e$ height are each set equal to the experimental peak width 46 meV. Visually, the sum seems to be a single smooth peak. We then apply our Gaussian fitting program to this artificial peak. The result is a fit, whose center is between the two generating Gaussians, displaced from the higher peak by $\frac{1}{3}$ of the original separation. Hence, we conclude that we should weight the various transitions by their strengths and calculate the correction required to go from the center of the resulting peak to the specific transition of interest.

The O^- photodetachment peak consists of six transitions between the two fine structure states of O^- $^2P_{1/2,3/2}$ and the three fine-structure states of O $^3P_{0,1,2}$. Far above threshold the obvious choice of weighting factors for these transitions is the product of the degeneracies of the initial and final states. Lineberger and Woodward, in a study of S^- photodetachment, [27] conclude that *at threshold* a slightly different weighting scheme is required. Table II shows that the calculation using a set of weighting factors suggested by Rau and Fano[36] is appropriate to the Lineberger-Woodward results as well as to the statistical weighting scheme used by Branscomb *et al.*[15] The energy levels and the value of the electron affinity, 1.465 ± 0.005 eV, are from Branscomb *et al.*[15]

The Branscomb *et al.* and the Rau-Fano weighting systems produce essentially the same numerical result. We find that the O^--peak center corresponds to an electron energy ~1.8 cm^{-1}, or 0.22 meV, less than the electron energy corresponding to the affinity. Thus we can use the O^- peak as an energy benchmark and assign it an "effective electron affinity" of 1.465 eV since the actual peak position differs from this value by a negligibly small energy.

B. NO Spin-Orbit Splitting and Rotational Corrections

The NO^- electronic state is isoelectronic with, and assumed to have the same configuration as, the O_2 $X\,^3\Sigma_g^-$ ground state.[32] Thus NO^- has two equivalent detachable electrons, each in a Π state, "counter rotating," but with parallel spins. After photodetachment, the final NO molecule is left in either the $^2\Pi_{3/2}$ or $^2\Pi_{1/2}$ state, depending on whether the removed electron spin was, in independent particle language, parallel or antiparallel to its orbital angular momentum. The spin-orbit energy

TABLE II. O^- transition weighting.

Transition	Energy from electron affinity (cm^{-1})	Statistical weights	Rao and Fano
$^2P_{1/2}$-$^3P_2$ (threshold)	−230	1.0	1.0
$^2P_{1/2}$-$^3P_1$	−71.5	0.6	1.8
$^2P_{1/2}$-$^3P_0$	−3.5	0.2	0.8
$^2P_{3/2}$-$^3P_2$ (electron affinity)	0	2.0	5.0
$^2P_{3/2}$-$^3P_1$	158.5	1.2	1.8
$^2P_{3/2}$-$^3P_0$	226.5	0.4	0.4
Correction (weighted average, cm^{-1})		+1.3	+2.2

difference between the $^2\Pi_{3/2}$ and $^2\Pi_{1/2}$ states is 121.1 cm^{-1}.[37] Since each fine-structure state is doubly degenerate we expect to see transitions to each with equal probability. We also expect that there will be P, Q, and R rotational branches for each final state. As for O^-, we list all of the possible transitions, assign each a relative intensity and calculate the final peak shape by folding in the electron analyzer function. In this way we find the relationship between the final peak center and the transition between the NO^- $^3\Sigma^-$ ($N=0, J=1$) state and NO $^2\Pi_{1/2}$ ($J=\frac{1}{2}$) state, from which we can determine the electron affinity.

We assume our transitions obey the selection rules $\Delta J = 0, \pm 1$ (Q, R, and P branches). At the photon energy we use, the outgoing electron is predominantly s wave and only at the highest electron energies does the other allowed channel, the d wave, become non-negligible. The final state of the NO is determined by considering the complex formed by the neutral NO and the outgoing s-wave electron in accordance with the selection rules. For example, for the final state $^2\Pi_{1/2}$ and a $\Delta J = 0$ (Q branch) transition, the NO molecule will be left with its total angular momentum to $J'' \pm \frac{1}{2}$, where J'' is the total angular momentum for the initial NO^- state. The two possible final states are due to two ways of coupling the outgoing electron's spin into the total angular momentum. Similar relationships exist for the P and R branches.

The total spin-orbit and rotational correction is obtained by first calculating the positions of the three branches for each final rotational state according to the selection rules just discussed. The origins of the two systems are appropriately displaced, with the $^2\Pi_{3/2}$ state lying 121.1 cm^{-1} (the spin-orbit splitting) above the $^2\Pi_{1/2}$ state. The intensity of rotational transition is then calculated. Each transition strength is multiplied by the Boltzmann factor

$$(2J''+1)\exp\left[-J''(J''+1)B_e''/kT\right] ,$$

where B_e'' is the rotational constant, T is the assumed rotational temperature, and J'' is the initial rotational angular momentum of the ion.

The P, Q, and R branches are next weighted relative to each other. The relative branch weights are the same for the $^2\Pi_{1/2}$ and $^2\Pi_{3/2}$ states. We have no good criterion for determining the relative strength of the P, Q, and R branches in photodetachment, but we feel that the ratio 1:2:1 is the most probable. Thus we have investigated this case and what we consider to be two extremes, 1:10:1 and 1:0:1. For each value of J'' we calculated the energy corresponding to the transitions of all three branches of both fine-structure states. The intensity is given by the Boltzmann factor times the assumed weighting factor for that branch. Each transition is then broadened by the numerically generated instrument function of the electron energy analyzer. This process is repeated for each value of J''. All of the intensities are finally summed. The result is a plot of intensity vs energy which is a slightly asymmetric Gaussian-shaped peak. This is the same peak shape we observe in the experiment. The rotational-spin-orbit correction is the energy difference between the energy at the center of this peak and the band origin of the $^2\Pi_{1/2}$ state, which we read from the graph. Table III gives the results of a series of these calculations. As shown by the first three lines of Table III, the three different choices for the relative intensities of the P, Q, and R branches produce the same correction to within 0.6 meV.

TABLE III. Rotational spin-orbit correction.

Maximum J''	Temperature	Weighting factors P	Q	R	Rotational spin-orbit correction (cm^{-1})	(meV)
36	630	1	0	1	−96	−11.9
36	630	1	10	1	−100	−12.4
36	630	1	2	1	−101	−12.5
36	530	1	2	1	−94	−11.6
36	730	1	2	1	−104	−12.9
12	630	1	2	1	−67	−8.3

The temperature of 630 °K used in these calculations is an experimental measurement of O_2^- vibrational temperature, the O_2^- being produced simultaneously with the NO^-. Since O_2^- can support excited vibrational states and since it is possible to obtain the relative populations of these states from the photodetachment data, a source temperature can be calculated assuming a Boltzmann distribution. We assume equal rotational and vibrational temperatures and use the temperature of 630 °K, determined from the O_2^- data, as an estimate of the rotational temperature for both NO^- and O_2^-. We investigated the effect an error of ±100 °K in the rotational temperature would have on the rotational spin-orbit correction. The results of our calculation for 530 and 730 °K are shown in lines four and five of Table III with the weighting we think most probable.

Although we have included values of J'' extending to 36, we note that for values of J'' greater than 12, NO^- is metastable against autodetachment to the $^2\Pi_{1/2}$ rotational ground state of NO. We think it unlikely, given our source conditions, that this situation could have a significant effect on the rotational distribution of NO^-, but to see how big an effect is possible, we make the drastic assumption that the rotational distribution of the ground state is cut off at $J''=12$. The results of this calculation are also shown in Table III.

We finally conclude that in order to take into account the rotational energy of the ions and neu-

TABLE IV. Summary of electron affinity data.

Transition $(v',0)$	Measured kinetic-energy difference (eV)	E_{vd}^{T} $(v',0)$ (eV)	E_{vd}^{T} (0,0) (eV)
(4,0)	−0.5317	0.9401	0.0324
(3,0)	−0.7512	0.7206	0.0346
(3,0)	−0.7536	0.7182	0.0322
(2,0)	−0.9779	0.4939	0.0331
(2,0)	−0.9764	0.4954	0.0346
(2,0)	−0.9788	0.4929	0.0321
(1,0)	−1.2075	0.2643	0.0322
(1,0)	−1.2076	0.2642	0.0321

trals and the spin-orbit splitting of the final state, 12.5 meV must be subtracted from the nominal value of the electron affinity E_{vd}^{T} (NO(0, 0)NO$^-$). We feel that the 1:2:1 weighting scheme is the most probable, and we use the other results in Table III in estimating possible systematic errors.

C. Calculation of Electron Affinity

We now assemble the results of all of the measurements and calculations discussed above to determine E_{vd}^{T} (NO(0, 0)NO$^-$), and reduce it to the electron affinity of NO. We have made multiple measurements of O$^-$-NO$^-$ energy differences. Table IV presents the results of these measurements, made over a period of 1 yr. To minimize the error in our results we calculate the electron affinity based on data for the NO(4, 0)NO$^-$ transition shown at the top of Table IV. The measured kinetic-energy difference is the smallest of the group and this minimizes the effect of the ± 0.005 systematic error present in the 1.030 scale correction factor. The other determinations listed in Table IV have higher error estimates and should be considered as checks on the result obtained from the NO(4, 0)NO$^-$ data.

The first step in the data reduction is the calculation of the vertical detachment energy for the transition. For the NO(4, 0)NO$^-$ transition, we have, using Eq. (8), and the appropriate numbers

$$E_{vd}^{T}(\mathrm{NO}(4,0)\mathrm{NO}^-) = 1.465 + (-0.5317) + 680.0\times\left(\tfrac{1}{16}-\tfrac{1}{30}\right)1836 = 0.9441\ \mathrm{eV}\ . \quad (24)$$

The value 1.465 eV used here is the "effective electron affinity" of O as calculated in Sec. VIII A. The result of this calculation is shown in the third column of Table IV.

The vertical detachment energy E_{vd}^{T} (NO(4, 0)NO$^-$) is then reduced to E_{vd}^{T} (NO(0, 0)NO$^-$) by subtracting the spectroscopically determined energy difference between the NO $^2\Pi(v=4, J=12)$ level and the NO $^2\Pi(v=0, J=12)$ level. The value of J equal to 12 is chosen as being typical at our source temperature although the energy difference is quite insensitive to the actual value of J selected. The result of this calculation, shown in the last column of Table IV, need only be corrected by the rotational-spin-orbit correction to yield the electron affinity. By applying the −12.5-meV rotational-spin-orbit correction to the NO(4, 0)NO$^-$ data we obtain a value of 24 meV for the electron affinity of NO. We emphasize that this electron affinity is the energy difference between the NO$^-$ $^3\Sigma^-$ vibrational and rotational ground state and the NO $^2\Pi_{1/2}$ vibrational and rotational ground state.

IX. ERROR ESTIMATES

A. Directly Measured Quantities

1. Peak Areas

Relative peak areas are tabulated in the form of the ratio of adjacent peak areas. This minimizes the propagation of both statistical and systematic errors across the data set.

a. Statistical errors. The peak area is calculated analytically, when the asymmetry in peak shape is negligible, from the values of the height and width determined for the best fit by the least-squares-fitting program. A good estimate of the statistical error in the area determination is then obtained from the error estimates for the height and width parameters. The fractional error estimate for each of these parameters is generally less than 1%. Hence, an error estimate of ± 2% for the statistical uncertainty present in the area determination is used.

The use of an analytic expression in the calculation of the area is justified by the fact that the fitted curve shows no systematic deviations from the data and the direct integration of the data produces results in agreement with the analytic results to better than ± 2%.

Figure 5 illustrates the variation in peak area as a function of the fitting parameters and also the sensitivity of the residuals to changes in each parameter.

b. Systematic errors. A systematic error in the determination of relative cross sections for vibrational transitions can arise if the electron energy analyzer has a transmission dependent upon transmission energy. An extremely pessimistic assumption would be a transmission function which was zero at zero electron energy and rose to unity at 2.5 eV. The flatness of the background counting rate in the region of interest suggests that our transmission problem must be much weaker than the one in this pessimistic model.

In order to be cautious in stating error estimates on intensity-dependent results we assume an approximately 50% change in transmission between

the high- and low-energy ends of our spectra. To do this we assume that the transmission is unity at the center of the spectra in question, 0.75 at the low-energy limit, 1.25 at the high-energy limit, and linear in between. The peak intensities are then corrected for this hypothetical transmission factor. To investigate the other extreme we use the same rate of change of transmission factor, but assume that the transmission is higher at the low-energy end of our spectra. Error estimates are obtained from the calculation of the effect each transmission function has on the relative peak heights, and ultimately on the values we obtain for ω_e'' and r_e''.

2. Peak Centers

Peak centers are determined by the fitting program in terms of (fractional) multichannel-analyzer channel numbers. The conversion gain of the analyzer is checked before and after each data run by sampling of precisely generated voltages at 0.1-V intervals across the range of interest. Differences in peak centers, in volts on the interaction chamber, are obtained as the product of difference in fit centers, conversion gain, and calibration factor.

a. Statistical errors. The statistical error, one standard deviation, in the location of the peak center is obtained from the nonlinear-least-squares-fitting program. The error is generally quite small, typically ± 0.3 meV. The behavior of the residuals of the fit as the center is forced from its optimum value is shown in Fig. 5.

b. Systematic errors. The only systematic error possible in the determination of the peak center could come about if the slightly asymmetric Gaussian function were not a good representation of the actual peak shape. We have found that our form gives a very good fit to the data (see Fig. 7). In no part of the peak do we see a systematic variation in the residuals of the fit indicating that if the functional form is incomplete then the effect of the error is small when compared with statistical errors.

3. Angular Distribution Constants

a. Statistical Errors. The fitting program determines the standard-deviation error limits on the angular distribution constant β, and these are indicated in Table I, along with the measurements. These statistical errors are typically about 1% of the measured value.

b. Systematic Errors. We have already discussed, in Sec. III H, how our method of handling the data compensates for the major source of systematic error, i.e., terms periodic in the half-wave-plate rotation frequency, or half the polarization rotation frequency. The fitting procedure also shows that the amplitude of terms periodic in frequencies greater than the polarization frequency are insignificant.

A residual source of systematic error may come from an incorrect determination of the background counting rate, which would be interpreted as an incorrect isotropic component in the angular distribution. As described in Secs. III E and III F, we have carefully established that signal and signal plus background channels are equivalent, i.e., yield balanced counting rates when no signal is present.

Similarly, deviation of the laser from complete linear polarization would systematically affect the angular distribution data. Appropriate checks have shown such deviation to be negligible.

Thus we assign negligible systematic error to the angular distribution measurements.

B. First Reduction

1. Relative Cross Section

a. Neglecting possible transmission error. Relative total cross sections are obtained from peak areas and angular distributions from Eq. (13), in which each area, measured at the maximum of an angular distribution, is normalized by $(1-\frac{1}{2}\beta)$. The appropriate weighting factors for a root-mean-square combination of the individual fractional errors are 1 for $\Delta A/A$, and $\beta/(2-\beta)$ for $\Delta\beta/\beta$. The resulting error in the cross-section ratio determination, using 2% for $\Delta A/A$ and 1% for $\Delta\beta/\beta$, is

$$\frac{\Delta(\sigma/\sigma')}{(\sigma/\sigma')} \approx 3\% \ ,$$

where σ, σ' refer to adjacent peaks.

b. Including a large transmission error. Since we believe the transmission error to be small, we state our relative cross sections with errors as determined by statistical considerations, as discussed in the above paragraph. In using these observed cross sections as experimental Franck-Condon factors to obtain the molecular constants, we make the pessimistic assumption that the transmission function changes by 50% of its average value across the range of the NO^- photodetachment peaks. For the lowest electron energy peaks, this is equivalent to assuming $\Delta(\sigma/\sigma')/(\sigma/\sigma') \approx 20\%$, and for the highest electron energy peaks, it is equivalent to assuming $\Delta(\sigma/\sigma')/(\sigma/\sigma') \approx 10\%$.

2. Energy-Difference Measurements

We have discussed, in Sec. IX A 2, possible statistical errors in determining the centers of the observed peaks. If only statistical errors were present, the determination of the energy difference between two peaks would have a typical standard deviation of 0.4 meV. The major error is systematic, and has its origin in the energy-scale correlation factor used in these experiments.

The correction factor used here is 1.030 with a

conservative error estimate of ±0.005. The error in the scale factor translates into a possible systematic error of approximately ±0.5% in the energy difference derived following scale correction.

A second systematic error occurs because we have not corrected the peak locations for the change in rotational energy of the neutral NO molecule as the outgoing d-wave channel becomes appreciable with higher outgoing electron energy. As we look at transitions to progressively lower final vibrational states the effect grows larger and the peak separations become slightly larger. If we were to use the comparison of the measured vibrational intervals with their spectroscopic counterparts as a means of measuring our energy-scale factor, we would conclude that the scale correction was decreasing with increased electron energy. As can be seen from Fig. 11 there seems to be a systematic decrease in the scale factor at higher electron energy.

Our scale-factor measurements are made at lower electron energies, where the d-wave component is small, and we apply the scale factor only in this range. Hence, we note this effect to explain the apparent systematic variation of our scale factor at high electron energies, but we work in a region where we need not consider the effect.

Since the zero of our energy scale is determined by measuring the energy difference between a calibration ion (O^-) and a known transition in the NO^- system, and there is a fixed 0.5% error in this energy difference, it is clear that the smallest possible energy difference should be selected for precise measurement. Other factors, such as the sensitivity of each transition to mechanical misalignments and the signal-to-noise ratio possible with each transition, contributed to the selection of the particular transition used for the electron affinity measurement.

C. Molecular Constants

The Franck-Condon-factor fitting technique, in which the negative ion r_e'' and ω_e'' are adjusted to yield an optimum (weighted least-squares) fit to the observed values of the relative cross section, is sensitive to changes of r_e'' of 0.001Å and changes of ω_e'' of 1%. That is, within this region of the $r_e'' - \omega_e''$ plane, the fit to the data is about equally good (with respect to falling within the statistical error bars on the observed relative cross sections). Figure 12 illustrates how good this fit actually is.

This sensitivity is not a valid indication of how well we have determined ω_e'' and r_e'', because a possible transition effect would cause a systematic error in our determination of the cross sections. To test and allow error estimates for this effect, we have differentially attenuated, by ±25%, the photodetachment spectrum of NO^-, and used the attenuated cross sections to compute outside limits for ω_e'' and r_e''.

We conclude that the transmission effect, in this worst case, could introduce a 0.010-Å error in r_e'' and a 14% error in ω_e''. Thus we state

$$r_e'' = 1.258 \pm 0.010 \text{ Å}$$

and

$$\omega_e'' = 1470 \pm 200 \text{ cm}^{-1} = 0.182 \pm 0.023 \text{ eV}.$$

Since, from Eq. (22)

$$\Delta B_e''/B_e'' = 2\Delta r_e''/r_e'' = 1.6\% ,$$

we obtain

$$B_e'' = 1.427 \pm 0.02 \text{ cm}^{-1} = 0.177 \pm 0.003 \text{ meV}.$$

D. Electron Affinity

1. Rotational-Spin-Orbit Corrections

The rotational-spin-orbit correction has been calculated for a number of different assumptions (see Table III). We feel that the 1:2:1 ratio of intensities of the P, Q, and R branches is the most likely. If the weighting are 1:10:1 the error introduced would be +0.1 meV and if it were 1:0:1 the error would be +0.6 meV. An error estimate of +1.0 and −0.4 meV should cover our uncertainty about which weighting scheme is proper.

The rotational temperature used in this calculation comes from a source-temperature determination made in the O_2^- experiment. In Table III, we consider the effect of an error of ±100 °K on the rotational-spin-orbit correction and arrive at error estimates of +0.9 and −0.4 meV.

Also considered in Table III is the possibility that the NO^- rotational levels lying above the NO rotational ground state were depopulated in the source. It seems highly unlikely that the ions could efficiently give up the 11 or more units of angular momentum required, but as a limiting case we calculate the effect upon the rotational-spin-orbit correction of cutting off the rotational distribution above $J'' = 12$. We find that if this were the case, an error of +4.2 meV would be present.

2. Measurement Errors

The combined statistical error present in the center-to-center measurement of the NO(4, 0)NO^--O^- energy difference is ±0.6 meV (one standard deviation). In addition the scale correction factor could introduce an error as large as ±0.5% of the energy difference or ±2.7 meV. The H-D measurements described in Sec. IV A limit any error due to mechanical misalignment to less than ±0.6 meV.

A summary of error estimates is presented in Table V. We total the errors presented to obtain an over-all error estimate of +10 and −5 meV.

The other determinations shown in Table IV

TABLE V. Summary of error estimates.

	Error estimate (meV)	
Rotational correction	+1.0	−0.4
Rotational temperature	+0.9	−0.4
No high values of J''	+4.2	−0.0
Peak center (statistical)	+0.6	−0.6
Scale correction factor	+2.7	−2.7
Mechanical misalignment	+0.6	−0.6
Total	+10.0	−4.7

produce a mean value of the electron affinity of 24.4 meV, with a standard deviation of ±1.1 meV. These measurements should carry higher error estimates because of the ±0.5% scale-factor error. The fact that they agree so well with the best measurement indicates that we have been conservative in our estimation of the size of the possible scale correction error.

Our final value $E_A(\mathrm{NO}) = 24^{+10}_{-5}$ meV is based upon the Branscomb *et al.*[15] value of 1.465 eV for the electron affinity of O. Any future change in the value of the electron affinity of O should be reflected additively in our value.

X. COMPARISON WITH THEORY AND OTHER EXPERIMENTS

A. Theory

Gilmore,[32] on the basis of extrapolations on isoelectronic series, has predicted $E_A(\mathrm{NO}) = 0.1$ eV. In view of the then accepted experimental results, it is remarkable that a theoretical treatment produced a value that agrees so well with ours. Gilmore's value for r_e'', from which, by Badger's rule, a value for ω_e'' may be estimated, also agrees well with our result.

We are not aware of any other theoretical analysis of the nitric oxide electron affinity.

B. Experiment

1. Other Electron Affinity Measurements

Farragher *et al.*[38] report a value of 0.9 ± 0.1 eV, from the slope of the logarithmic ratio of electron to ion currents vs reciprocal temperature of a hot filament. This is the most-frequently tabulated value for $E_A(\mathrm{NO})$.

Stockdale *et al.*[39] report a lower bound of 0.65 eV, from the threshold energy for the appearance of NO^- from NO_2^- electron collisions.

Lacmann and Herschbach[40] have recently reported a measurement of the electron affinity via the collisional ionization of fast K atoms by NO molecules. They report an electron affinity ≈0.

Berkowitz *et al.*[41] have studied the endothermic charge-transfer reaction with I^- and concluded that $E_A(\mathrm{NO}) \geq 0.09 \pm 0.1$ eV.

We find that we are in excellent agreement with the last two determinations.

2. Electron-Scattering Measurements

As mentioned earlier, the trapped-electron method has been used by Spence and Schulz[30] to obtain a value of 0.170 eV for ω_e'' and 1.00 ± 0.25 meV for $\omega_e x_e''$. They then calculate r_e'' from Badger's rule and obtain 1.286 Å for r_e''. Although their technique cannot measure the electron affinity, they find, by assuming that the electron affinity is near zero, that an affinity of 0.050 eV is in agreement with their data.

Our results indicate a value of $r_e'' = 1.258 \pm 0.010$ Å. Considering that Badger's rule has been found[42] to be good in most cases to about ±5%, the agreement is as good as can be expected. Our value of ω_e'' is 182 ± 23 meV and theirs is 170 ± 20 meV.[30,43] We do not determine a value of $\omega_e x_e''$. The estimate of the electron affinity made by Spence and Schulz comes from an extrapolation of the vibrational levels observed using their measured value of ω_e''. This estimate does not consider the spin-orbit splitting of the NO ground state or the rotational correction. This result is clearly in agreement with ours.

The photodetachment technique and the electron-scattering method are complementary ways of investigating negative-ion structure. The electron-scattering method can directly determine $\omega_e x_e''$ and, given the electron affinity, determine ω_e''. The photodetachment technique measures the electron affinity, r_e'', and ω_e''. In this case the results of the two techniques are in excellent agreement.

XI. CONCLUSIONS AND SUMMARY

We have shown that laser photodetachment and photoelectron spectrometry can provide precise information about molecular-electron affinities and molecular-negative-ion spectroscopic constants. Measured electron energy peaks provide vertical detachment energies between negative-ion and parent neutral molecule. Their intensities (corrected by the measured photoelectron angular distributions) provide experimental relative Franck-Condon factors for the observed initial-final vibrational-state pairs; the negative-ion spectroscopic constants are determined as parameters of the ionic rotational-vibrational wave functions yielding best overlap integral fits to these data. The vertical detachment energy corresponding to the ground vibrational states of ion and molecule, and the spectroscopic constants of the ion, determine the molecular electron affinity.

We have solved the problem of identifying the vibrational states corresponding to the observed transitions. We have shown that the photoelectron spectrum originating on the zeroth negative-ion vibrational state may be identified by its property of a single maximum in its Franck-Condon-factor envelope with the series of final molecular vibrational states. We have shown that there are several methods for uniquely identifying the final vibrational states observed, an important one being the comparison of photoelectron spectra from isotopically labeled molecular negative ions.

Finally, we have identified and corrected for the role of molecular rotation in causing vertical detachment energies to differ from electron affinities.

ACKNOWLEDGMENTS

We are indebted to Dr. V. Cermak for suggesting the use of N_2O as a source gas. The ion optical design is to be credited to Dr. B. Brehm, and the electron energy analyzer was designed with the assistance of Dr. C. Kuyatt. The apparatus was constructed with the help of C. Pelander, E. Logan, D. Hendry, and R. Weppner. Dr. D. L. Albritton, Dr. A. L. Schmeltekopf, and Dr. R. N. Zare are to be thanked for many helpful discussions and for making available to us their diatomic Franck-Condon-factor programs prior to their publication. Finally, we are indebted to Dr. L. M. Branscomb, Dr. W. C. Lineberger, Dr. H. Broida, Dr. F. Mies, and Dr. A. V. Phelps for many lively discussions during the course of the work.

---

†Paper based in part on a thesis submitted by M. W. Siegel to the University of Colorado, in partial fulfillment of the requirements for the Ph. D. degree. Work supported by the Advanced Research Projects Agency, The Department of Defense, and was monitored by U. S. Army Research Office—Durham, Box CM, Duke Station, N. C. 27706, under Contract No. DA-31-124-ARO-D-139.

*Present address: Department of Aerospace Engineering and Engineering Physics, University of Virginia, Charlottesville, Va.

‡Present address: Optical Physics Division, National Bureau of Standards, Gaithersburg, Md.

§Staff member, Laboratory Astrophysics Division, National Bureau of Standards.

¶Staff member, Quantum Electronics Division, National Bureau of Standards.

[1]L. M. Branscomb, in *Advances in Electronics and Electron Physics*, edited by L. Marton (Academic, New York, 1957), Vol. 9, pp. 43–94.

[2]L. M. Branscomb, in *Atomic and Molecular Processes*, edited by D. R. Bates (Academic, New York, 1962), pp. 100–140.

[3]S. J. Smith, in *Methods of Experimental Physics*, edited by L. Marton (Academic, New York, 1968), Vol. 7A, pp. 179–208.

[4]B. Brehm, M. A. Gusinow, and J. L. Hall, Phys. Rev. Letters 19, 737 (1967).

[5]H. S. W. Massey, *Negative Ions*, 2nd ed. (Cambridge U.P., London, 1950).

[6]B. L. Moiseiwitsch, in *Advances in Atomic and Molecular Physics*, edited by D. R. Bates and I. Estermann (Academic, New York, 1965), Vol. I.

[7]R. J. Celotta, R. A. Bennett, J. L. Hall, M. W. Siegel, and J. Levine, following paper, Phys. Rev. A 6, 631 (1972).

[8]E. U. Condon, Am. J. Phys. 15, 365 (1947).

[9]L. M. Branscomb, Phys. Rev. 148, 11 (1966).

[10]E. M. Purcell, Phys. Rev. 54, 818 (1939).

[11]C. E. Kuyatt and J. A. Simpson, Rev. Sci. Instr. 38, 103 (1967).

[12]J. L. Hall and M. W. Siegel, J. Chem. Phys. 48, 943 (1968).

[13]J. Cooper and R. N. Zare, J. Chem. Phys. 48, 942 (1968).

[14]S. J. Smith and D. S. Burch, Phys. Rev. 116, 1125 (1959).

[15]L. M. Branscomb, D. S. Burch, S. J. Smith, and S. Geltman, Phys. Rev. 111, 504 (1958).

[16]This is always the case if the negative-ion ground state is a spin-orbit multiplet; see Ref. 18, Fig. 1.

[17]S. T. Manson, Phys. Rev. Letters 26, 219 (1971). This reference repeats the form of β given in Ref. 16, and discusses how the same β determines the photoelectron angular distribution about the photon direction when unpolarized photons are used.

[18]D. S. Burch and S. J. Smith, Phys. Rev. 112, 171 (1958).

[19]G. Herzberg, *Molecular Spectra and Molecular Structure*, Vol. 1 (Van Nostrand, New York, 1950), Chaps. II and III.

[20]Obtained from Allegheny Ludlum Steel Corp., Brackenridge, Pa. 15014.

[21]The least-squares-fitting programs are based on R. H. Moore and R. K. Zeigler, Report No. LA-2367 (Los Alamos Scientific Laboratory, 1960) (unpublished).

[22]The programs RKR, FCF, and MORSE have been generously provided by D. L. Albritton, A. L. Schmeltekopf, and R. N. Zare prior to their publication [in Diatomic Intensity Factors (Harper and Row, New York, to be published)].

[23]P. M. Morse, Phys. Rev. 34, 57 (1929).

[24]J. L. Dunham, Phys. Rev. 34, 446 (1929).

[25]M. W. Siegel, thesis (University of Colorado, 1970) (unpublished).

[26]R. J. Celotta, M. W. Siegel, J. L. Hall and J. Levine, Bull. Am. Phys. Soc. 15, 326 (1970) (note that NO electron affinity is a misprint); 15, 1515 (1970); 16, 212 (1971).

[27]W. C. Lineberger and B. Woodward, Phys. Rev. Letters 25, 424 (1970).

[28]Reference 19, p. 201.

[29]J. L. Dunham, Phys. Rev. 41, 721 (1932).

[30]D. Spence and G. J. Schulz, Phys. Rev. A 3, 1968 (1971).

[31]D. A. Albritton has communicated to us the NO $X\,^2\Pi$ molecular constants selected for use in Ref. 26. We use, after weighting, $\omega_e = 1904.104\ \text{cm}^{-1}$, $\omega_e x_e = 14.087\ \text{cm}^{-1}$, $B_e = 1.7048\ \text{cm}^{-1}$, and $r_e = 1.150\,79$ Å.

[32]F. R. Gilmore, J. Quant. Spectry. Radiative Transfer 5, 369 (1965).

[33]R. M. Badger, J. Chem. Phys. 2, 129 (1934); 3, 710 (1935).

[34]E. Hutchisson, Phys. Rev. 36, 410 (1930).
[35]Reference 19, p. 106.
[36]A. R. P. Rau and U. Fano, Phys. Rev. A 4, 1751 (1971).
[37]Reference 19, p. 558.
[38]A. L. Farragher, F. M. Page, and R. C. Wheeler, Discussions Faraday Soc. 37, 205 (1964).
[39]J. A. D. Stockdale, R. N. Compton, G. S. Hurst, and P. W. Reinhardt, J. Chem. Phys. 50, 2176 (1969).
[40]K. Lacmann and D. R. Herschbach, Chem. Phys. Letters 6, 106 (1970).
[41]J. Berkowitz, W. A. Chupka, and D. Gutman, J. Chem. Phys. 55, 2733 (1971).
[42]Reference 19, pp. 457–459.
[43]G. Schulz (private communication).

PHYSICAL REVIEW A VOLUME 6, NUMBER 2 AUGUST 1972

Molecular Photodetachment Spectrometry. II. The Electron Affinity of O_2 and the Structure of O_2^-†

R. J. Celotta,* R. A. Bennett, J. L. Hall,‡ M. W. Siegel,§ and J. Levine‖
Joint Institute for Laboratory Astrophysics, Boulder, Colorado 80302
(Received 12 October 1971)

A beam of O_2^- ions, extracted from a glow discharge in N_2O, is crossed with the linearly polarized intracavity photon beam of an argon-ion laser (4880 Å). Electrons photodetached at right angles to the crossed beams are energy filtered by a hemispherical analyzer. The electron energy spectra are characteristic of photodetachment from the $v'=0$ state of O_2^- to the $X\,^3\Sigma_g^-$ and $a\,^1\Delta_g$ states of O_2. Vibrational state analysis is facilitated by the use of isotopes. The electron affinity obtained is 0.440 ± 0.008 eV. Additionally, we have measured the relative transition probabilities as a function of final vibrational state and the angular distributions of the outgoing electrons. The relative intensities, corrected by the angular distributions, determine through Franck-Condon-factor analysis the internuclear distance for the negative ion. We find $r_e'' = 1.341 \pm 0.010$ Å and therefore $B_e'' = 1.17 \pm 0.02$ cm^{-1}.

I. INTRODUCTION

Reactions involving molecular oxygen and its negative ion are of primary importance in understanding air chemistry, particularly in understanding D-region composition and processes. It is therefore not surprising that there is currently a great deal of interest in the electron affinity of molecular oxygen. There is a notably long history of O_2 electron-affinity determinations. Figure 1 shows all the determinations known to us plotted against their approximate publication date. Let us review briefly the techniques that produced these values.

The first determination of the O_2 electron affinity was made by Loeb.[1] Loeb determined the attachment energy by observing the energy required for detachment when an ion collides with a neutral molecule in a swarm-type experiment. His value of 0.34 eV is an upper limit. Bloch and Bradbury[2] used a model fitted to then current experimental data to arrive at an upper limit for the electron affinity of 0.17 eV. Massey[3] used rules for formulated by Mulliken,[4] to arrive at an electron affinity of about 1 eV. Since his argument assumed the electron affinity of O to be 2.2 eV, and we now know that it is 1.465 eV,[5] we can correct his predicted value to 0.27 eV. Pritchard[6] reviewing lattice energy calculations, concluded that 0.9 ± 0.1 eV was the most probable value for the electron affinity. Burch *et al.*[7] performed a photodetachment experiment and measured the cross section for photodetachment from O_2^- as a function of wavelength. Their measured cross section was found to be an excellent fit to the threshold form, derived by Geltman,[8] over an unexpectedly large region (0.4–2.5 eV). An extrapolation of the cross-section data to threshold provides a value of 0.15 eV for a detachment energy. By determining the appearance potential for the formation of O_2^- in a mass spectrometer, Curran[9] concluded that $E_A(O_2) \geq 0.58$ eV. Pack and Phelps[10] published a value of 0.46 eV obtained in a swarm-type experiment and later refined their value to 0.43 ± 0.02 eV. In these experiments the O_2^- ion had to survive approximately 10^8 collisions and was therefore expected to be in its lowest vibrational state. This value of the electron affinity (0.43 ± 0.02) eV has been the most widely accepted to date. Fischer *et al.*[11] studied charge transfer of H^- to O_2 and concluded that the electron affinity is greater than that of H (0.754 eV).[12] This experiment is contradicted by that of Dunkin *et al.*,[13] in which thermal charge transfer was not observed. Stockdale *et al.*[14] studied the dissociative attachment of electrons to NO_2 and from measured appearance potentials concluded that $E_A(O_2) \geq 1.1$ eV. However, depending on the calibration of the